HHS Public Access

Author manuscript

Nat Immunol. Author manuscript; available in PMC 2019 June 10.

Published in final edited form as:

Nat Immunol. 2019 January ; 20(1): 73–85. doi:10.1038/s41590-018-0274-0.

The transcription factor c-Maf is essential for the commitment of IL-17-producing γδ T cells

Matthew K. Zuberbuehler[1,2], **Morgan E. Parker**[1,2], **Joshua D. Wheaton**[1], **Jaclyn R. Espinosa**[1], **Harmony R. Salzler**[1], **Eunchong Park**[1], and **Maria Ciofani**[1,*]

[1]Department of Immunology, Duke University Medical Center, Durham, NC, 27710

[2]Equal contribution.

Abstract

γδ T cells that produce the cytokine IL-17 (Tγδ17 cells) are innate-like mediators of immunity that undergo effector programming in the thymus. While regulators of Tγδ17 specialization restricted to various Vγ subsets are known, a commitment factor essential to all Tγδ17 cells has remained undefined. In this study, we identified c-Maf as a universal regulator for Tγδ17 cell differentiation and maintenance. *Maf* deficiency caused an absolute lineage block at the immature $CD24^{+}CD45RB^{lo}$ γδ thymocyte stage, which revealed a critical checkpoint in the acquisition of effector functions. Here, c-Maf enforced Tγδ17 cell identity by promoting chromatin accessibility and expression of key type 17 program genes, notably *Rorc* and *Blk*, while antagonizing the transcription factor TCF1, which promotes IFN-γ-producing γδ T cells (Tγδ1 cells). Furthermore, γδ T cell antigen receptor (γδTCR) signal strength tuned c-Maf expression, which indicates that c-Maf is a core node connecting γδTCR signals to Tγδ17 cell transcriptional programming.

IL-17-producing γδ T cells (Tγδ17 cells) provide an immediate source of IL-17 at barrier sites, supporting pro-inflammatory immune function. As such, Tγδ17 cells exert non-redundant functions in bacterial and fungal immunity[1, 2], and the development of autoimmunity[3]. Unlike conventional αβ T cells, innate-like γδ T cells become functionally 'preprogrammed' during ontogeny in the thymus[4]. This generates effectors including type 1 γδ T cells (Tγδ1 cells) characterized by expression of IFN-γ and T-bet, and type 17 Tγδ17 cells defined by expression of IL-17A and RORγt.

*Correspondence for materials should be addressed to M.C. (maria.ciofani@duke.edu).

Author Contributions

M.K.Z, M.E.P, and M.C. designed, performed, and analyzed experiments. J.W. performed computational analyses of RNA-seq, ChIP-seq, and ATAC-seq data. H.R.S, J.R.E, and E.P. performed experiments. M.C. conceived the study and wrote the manuscript.

Data availability

Sequence data that support the findings of this study have been deposited in GEO with the primary accession code GSE120427. Other sequence data referenced in this study are listed in the methods.

Competing Interests

The authors declare no competing interests.

γδ T cell development begins in the fetus and occurs as successive 'waves' characterized by distinct Vγ usage. In mice, Vγ3$^+$ dendritic epidermal T cells (DETC) develop first and migrate to the skin[5], followed by Vγ4$^+$ T cells that seed the lung and female reproductive mucosa[6] (Vγ nomenclature as in[7]). Vγ2$^+$ and Vγ1$^+$ γδ T cells develop in the late fetal stages and throughout life. Tγδ17 cell specialization also occurs as a discrete functional wave from E16 to birth[8], and as such, Tγδ17 cells are enriched for Vγ4 and Vγ2 usage.

Both TCR-dependent and –independent mechanisms underlie γδ T cell effector commitment in the thymus. γδTCR signal strength plays a role such that strong ligand-induced signals drive the adoption of the Tγδ1 fate, whereas weaker, potentially ligand-independent, signals promote the Tγδ17 fate[9, 10, 11]. Additionally, thymic stromal-derived signals influence γδ T cell effector identity. Indeed, the Wnt-activated transcription factor TCF1 promotes Tγδ1 and limits Tγδ17 cell generation[12], whereas Notch-induced Hes1 and TGF-β signals are necessary for IL-17 production in γδ thymocytes[13, 14]. Additional complexity resides in the unique regulatory requirements of select γδ T cell subsets for effector specification. HEB and downstream targets, Sox4 and Sox13, are selectively essential for Tγδ17 differentiation of the Vγ2$^+$ subset of γδ T cells[12, 15], while PLZF controls the development of IL-17$^+$ Vγ4$^+$ γδ T cells[16]. A universal commitment factor that drives *Rorc* expression and type 17 programming in all γδ T cells remains unknown.

The AP-1 transcription factor, c-Maf is a pleiotropic regulator of T cell effector programming. c-Maf is essential for activation or repression of key cytokine loci in CD4$^+$ T cells[17, 18, 19, 20] and invariant NKT cells[21], and for the adoption of specialized effector phenotypes by regulatory T cells (T_{reg} cells)[22, 23]. Transcriptomic profiling of γδ thymocyte subsets identified c-Maf as highly co-expressed with *Rorc*[24], suggesting a function for c-Maf in γδ T cell specialization. Here, we identified c-Maf as a universal essential regulator of Tγδ17 differentiation, required by all Vγ subsets for the induction and maintenance of Tγδ17 cells. Specifically, c-Maf activated the chromatin accessibility and expression of key loci in the type 17 effector program (e.g. *Rorc, Il17a, Blk*), while antagonizing negative regulators of Tγδ17 differentiation such as TCF1 (*Tcf7*). Following γδ-selection, the induction and magnitude of c-Maf expression was tuned by the strength of γδTCR signaling, implicating c-Maf as a rheostat controlling effector γδ T cell generation.

Results

c-Maf is specifically expressed in Tγδ17 cells and progenitors

To explore the role for c-Maf in the Tγδ17 lineage, we evaluated the expression of c-Maf within the γδ T cell compartment. In the inguinal lymph nodes (iLN), spleen and small intestine lamina propria (SILP), high expression of c-Maf was restricted to RORγt$^+$ γδ T cells (Fig. 1a). RORγt$^+$ γδ T cells were also uniformly c-Maf^{hi} in the thymus, where a subset of mature Tγδ17 cells reside[8]. Conversely, Eomes$^+$, T-bet$^+$, CD27$^+$ or CD45RB^{hi} [4, 11] Tγδ1 cells lacked high expression of c-Maf (Fig. 1a, b), suggesting c-Maf selectively marks Tγδ17 cells.

In the FT, c-Maf protein was restricted to γδTCR$^+$ thymocytes, with low or no c-Maf detected for the early T cell precursor (ETP), CD4$^-$CD8$^-$ double negative 2 (DN2) and DN3

progenitor cell subsets, nor in $CD4^+CD8^+$ double positive (DP) cells (Fig. 1c). During fetal ontogeny c-Maf expression was first detected in post γδ-selection $CD25^+CD27^+$ progenitor cells and was increased as cells downregulate first CD25 and then CD27 to become $CD25^-CD27^-$ cells that are enriched for Tγδ17 cells[4] (Fig. 1d, Supplementary Fig. 1a, b). RORγt and c-Maf expression coincided starting at the $CD25^+CD27^+$ stage, suggesting RORγt is induced in c-Maf^+ precursors. Alternatively, expression of CD45RB, which is associated with DETC and Tγδ1 development[11, 25], delineated $CD45RB^{hi}ROR\gamma t^-$ and $CD45RB^{lo}ROR\gamma t^+$ FT γδ T cell subsets (Fig. 1e). We also detected a $CD45RB^{int}\gamma\delta TCR^{int}$ population that contained precursors for both $CD45RB^{hi}Eomes^+$ Tγδ1 and $CD45RB^{lo}ROR\gamma t^+$ Tγδ17 cells when cultured *in vitro* with OP9-DL1 bone marrow stromal cells (Supplementary Fig. 1c). Expression of c-Maf was lowest in $CD45RB^{hi}$ Tγδ1 cells, intermediate in $CD45RB^{int}$ cells, and highest in the $ROR\gamma t^+CD45RB^{lo}$ Tγδ17 subset (Fig. 1e). Thus, c-Maf is uniformly upregulated during Tγδ17 differentiation.

c-Maf expression was also restricted to $CD73^-$ γδ thymocytes (Fig. 1f), which include developing Tγδ17 cells[15], and was sustained in $ROR\gamma t^+$ Tγδ17 cells that transition to the mature $CD24^{lo}$ stage (Fig. 1f). Although *Maf* mRNA was reported as enriched in $V\gamma2^+$ thymocytes[24], we detected c-Maf^{hi} cells in a proportion of all Vγ subsets examined, especially in Vγ4-enriched cells (gated $V\gamma1^-V\gamma2^-V\gamma3^-$; Supplementary Fig. 1d), which are predominantly Tγδ17 cells[11]. Thus, the correlation between RORγt and c-Maf expression in developmental and adult peripheral γδ T cell populations suggested a critical function for c-Maf in Tγδ17 cells.

c-Maf is selectively required in peripheral Tγδ17 cells

We bred mice harboring a *Maf* conditional allele with mice expressing Cre recombinase from the *Il7r* locus ($Il7r^{Cre}$) to delete *Maf* in lymphoid cells[26, 27]. $Maf^{fl/fl}Il7r^{Cre}$ mice were indistinguishable from $Maf^{+/+}Il7r^{Cre}$ controls with respect to thymic proportions of DN progenitor T cells, or αβ and γδ T cells (Supplementary Fig. 2a). Deletion of *Maf* ablated the Tγδ17 cell population, as indicated by the complete loss of $ROR\gamma t^+$, $CCR6^+$, or IL-$17A^+$ γδ T cells in the spleen, iLN and SILP (Fig. 2a,b and Supplementary Fig. 2b). In particular, γδ T cells in the female reproductive tract (FRT) mucosa and dermal γδ T cells, which are primarily Tγδ17 cells, were absent in $Maf^{fl/fl}Il7r^{Cre}$ mice (Fig. 2b, c). In ~20% of $Maf^{fl/fl}Il7r^{Cre}$ mice, c-$Maf^+ROR\gamma t^+$ γδ T cells with non-deleted Maf^{fl} alleles were detected (Supplementary Fig. 2c) and excluded from analysis. Of note, the proportions and numbers of IFN-γ^+, $Eomes^+$ or T-bet^+ Tγδ1 cells were unaltered in $Maf^{fl/fl}Il7r^{Cre}$ mice (Fig. 2a,b and Supplementary Fig. 2b), and $\gamma\delta TCR^{hi}$ type 1-associated skin DETCs remained abundant (Fig. 2c), indicating c-Maf is selectively required for Tγδ17 cells. Moreover, other $ROR\gamma t^+$ subsets such as group 3 innate lymphoid cells (ILC3) and $CD4^+$ T_H17 cells were generated in $Maf^{fl/fl}Il7r^{Cre}$ mice (Supplementary Fig. 2d), highlighting a distinct c-Maf-dependence in γδ T cells for RORγt induction.

Although the representation of c-Maf^+ cells varies among Vγ subsets, the proportion of Vγ1, Vγ2, and $V\gamma1^-V\gamma2^-$ subsets was unchanged in thymic, splenic or iLN γδ T cells in $Maf^{fl/fl}Il7r^{Cre}$ versus $Maf^{+/+}Il7r^{Cre}$ mice (Supplementary Fig. 2e). However, at mucosal sites where γδ subsets are highly comprised of $ROR\gamma t^+$ Tγδ17 cells, such as $V\gamma4^+$ cells in the

FRT and V$\gamma2^+$ cells in the SILP, the distribution was significantly altered in *Maf*$^{fl/fl}$*Il7r*^{Cre} mice (Fig. 2, Supplementary Fig. 2e). Thus, non-T$\gamma\delta17$ V$\gamma2^+$ cells were unable to compensate for the absence of RORγt^+V$\gamma2^+$ cells in the SILP, potentially reflecting specialized niches for effector $\gamma\delta$ subsets in the SILP.

To evaluate the functional consequence of T$\gamma\delta17$ cell loss, we challenged *Maf*$^{+/+}$*Il7r*^{Cre} and *Maf*$^{fl/fl}$*Il7r*^{Cre} mice with cutaneous *Candida albicans* infection, for which both IL-17A and $\gamma\delta$ T cells are required for resistance[28]. Analysis of infected skin at day 3 showed that *Maf*$^{fl/fl}$*Il7r*^{Cre} mice had a 6-fold higher *C. albicans* burden compared to infected *Maf*$^{+/+}$*Il7r*^{Cre} mice (Fig. 2d), implicating c-Maf-dependent T$\gamma\delta17$ cells in controlling cutaneous *C. albicans* infection. Therefore, c-Maf is essential in the $\gamma\delta$ T cell lineage for type 17-associated phenotype and functions.

c-Maf is required for T$\gamma\delta17$ cell commitment during ontogeny

To assess the requirement for c-Maf in T$\gamma\delta17$ cell development, we analyzed thymi from *Maf*$^{+/+}$*Il7r*^{Cre} and *Maf*$^{fl/fl}$*Il7r*^{Cre} fetuses between E16 and E18. While expression of RORγt was detected in 40% of *Maf*$^{+/+}$*Il7r*^{Cre} $\gamma\delta$TCR$^+$ FT cells by E18, *Maf*$^{fl/fl}$*Il7r*^{Cre} $\gamma\delta$ thymocytes failed to induce high-level expression of RORγt (Fig. 3a, Supplementary Fig. 2b). The residual *Maf*$^{fl/fl}$*Il7r*^{Cre} RORγt^{lo} $\gamma\delta$ thymocytes (Fig. 3a) may reflect inefficient *Rorc* activation, or misdirected $\gamma\delta$TCR-mediated $\alpha\beta$ lineage differentiation. Indeed, RORγt expression in *Maf*$^{fl/fl}$*Il7r*^{Cre} $\gamma\delta$ T cells was similar to that of wild-type CD3ε^- DN cells (Fig. 3a) which are in transition to the DP stage. Notably, production of IL-17A (Fig. 3b), and the expression of Blk kinase (Fig. 3c), which is selectively required for the development of T$\gamma\delta17$ cells[29], was abrogated in *Maf*$^{fl/fl}$*Il7r*^{Cre} compared to *Maf*$^{+/+}$*Il7r*^{Cre} $\gamma\delta$ thymocytes. Downregulation of TCF1 characteristic of T$\gamma\delta17$ differentiation was also impaired, whereas the downregulation of CD45RB was unaffected (Fig. 3c). These results reveal a c-Maf-dependent T$\gamma\delta17$ effector specialization checkpoint at the CD45RB^{lo} stage. Reaggregate thymic organ cultures (RTOC) reconstituted with a mixture of *Maf*$^{fl/fl}$*Il7r*^{Cre} (CD45.2$^+$) and *Maf*-sufficient (CD45.1$^+$) DN2 thymocytes indicated the c-Maf-dependence for T$\gamma\delta17$ diversification was cell-intrinsic (Supplementary Fig. 3a).

Defects in T$\gamma\delta17$ differentiation result in the selective loss of V$\gamma2^+$ or V$\gamma4^+$ subsets[12, 15, 16]. We observed similar proportions of V$\gamma1^+$, V$\gamma2^+$ and V$\gamma3^+$ cells in *Maf*$^{fl/fl}$*Il7r*^{Cre} compared to control E17 FT (Supplementary Fig. 3b), indicating *Maf* deficiency did not affect the fetal Vγ distribution. However, the proportion of total mature CD24^{lo} $\gamma\delta$ thymocytes in *Maf*$^{fl/fl}$*Il7r*^{Cre} FT was decreased (Supplementary Fig. 3b). We focused the analysis on V$\gamma3^+$ and V$\gamma4^+$ thymocytes undergoing maturation before birth (Supplementary Fig. 3c). Whereas CD24 downregulation on T$\gamma\delta1$-enriched V$\gamma3^+$ cells was normal in *Maf*$^{fl/fl}$*Il7r*^{Cre} FT, T$\gamma\delta17$-associated V$\gamma4^+$ cells (gated V$\gamma1^-$V$\gamma2^-$V$\gamma3^-$) were arrested at the immature CD24^{hi} stage (Supplementary Fig. 3c). Thus, c-Maf is required for $\gamma\delta$ thymocytes to adopt the type 17 functional program and progress to the CD24^{lo} mature stage.

To determine the sufficiency of c-Maf in driving T$\gamma\delta17$ differentiation, fetal liver progenitor cells were differentiated into DN T cell precursors on OP9-DL1 cells, transduced with a c-Maf-expressing or empty retroviral vector, and purified DN3 cells were assessed for T$\gamma\delta17$

development following OP9-DL1 culture. c-Maf overexpression cultures showed a 2.7-fold increase in the proportion of RORγt^{+}CD45RB^{lo} γδ T cells relative to empty-virus cultures (Fig. 3d). A similar enhancement was observed when c-Maf-transduced FT γδTCR^{int}CD45RB^{int} γδ T cell precursors were differentiated in RTOC for 8 days (Supplementary Fig. 3d). Whereas empty-vector RTOCs displayed a Tγδ1-skewed potential for γδTCR^{int}CD45RB^{int} γδ T cell progenitors by generating mostly CD45RB^{hi} cells, c-Maf overexpression directed differentiation of mainly RORγt^{+}CD45RB^{lo} cells (Supplementary Fig. 3d). Notably, Tγδ17 lineage promotion by c-Maf was dependent on γδTCR expression as c-Maf-transduced *Rag1*$^{-/-}$ DN3 cells did not upregulate RORγt in OP9-DL1 culture, whereas transduction of γδTCR chains rescued type 17 differentiation among c-Maf^{+} cells (Fig. 3e). Together, these data indicate c-Maf is an essential commitment factor for Tγδ17 cell diversification.

Tγδ17 cells require continuous c-Maf expression

To assess the role of c-Maf in maintaining Tγδ17 identity, we bred *Maf*$^{fl/fl}$ mice to *Rorc*-Cre transgenic mice[30] to delete *Maf* in RORγt-expressing γδ T cells. Mature RORγt^{+} or IL-17A^{+} γδ cells were absent in the thymus and periphery of adult *Maf*$^{fl/f}$*Rorc*-Cre mice (Supplementary Fig. 4a). Development of Tγδ17 cells as a single wave during late fetal gestation permits the effect of c-Maf deletion to be evaluated in a semi-synchronized neonatal population. Depletion of c-Maf protein in *Maf*$^{fl/fl}$*Rorc*-Cre RORγt^{+} γδ thymocytes by day 2 (Fig. 4a and Supplementary Fig. 4b), resulted in a 2-fold reduction in the proportion and number of Tγδ17 cells relative to *Maf*$^{+/+}$*Rorc*-Cre (Fig. 4a and Supplementary Fig. 4c). The remaining *Maf*$^{fl/fl}$*Rorc*-Cre Tγδ17 thymocytes were RORγt^{lo} (Fig. 4a), lacked Blk expression and robust IL-17A production (Fig. 4b). As such, RORγt^{hi} Blk^{+} γδ thymocytes were absent in *Maf*$^{fl/fl}$*Rorc*-Cre, whereas the RORγt^{lo} Blk^{-} fraction was comparable to that of *Maf*$^{+/+}$*Rorc*-Cre controls (Fig. 4b), revealing a c-Maf-dependent checkpoint at this stage. Accordingly, *Maf* deletion resulted in enhanced apoptosis of Tγδ17 cells, evidenced by a 2-fold increase in AnnexinV^{+} RORγt^{+} γδ T cells in *Maf*$^{fl/fl}$*Rorc*-Cre *versus* control neonates (Fig. 4c). Furthermore, the retroviral-mediated restoration of Blk expression in *Maf*$^{fl/fl}$*Rorc*-Cre CD45RB^{lo} γδ thymocytes rescued the viability of these cells (Fig 4d and Supplementary Fig. 4d). Thus, Tγδ17 cells require c-Maf to maintain viability and lineage identity, including high expression of RORγt and Blk.

Maf directly regulates the *Rorc* locus

Motif analysis identified two Maf recognition elements (MARE) within a conserved noncoding sequence (CNS) located 10kb from the *Rorc(t)* transcription start site (TSS; CNS +10) (Supplementary Fig. 5). Chromatin immunoprecipitation (ChIP) assay of purified CD45RB^{lo} γδ fetal thymocytes indicated significant binding of c-Maf at CNS+10 relative to a negative control region (Neg-5; Fig. 5a). Consistent with previous ChIP-seq data[20], c-Maf bound predominantly 1.5kb upstream of the *Rorc(t)* TSS (CNS-1.5) and to a lesser degree at other CNS in *in vitro* polarized T_H17 cells (Fig. 5a), indicating c-Maf occupied distinct *cis* regions in the *Rorc* locus in γδ T cells compared to T_H17 cells.

To test whether CNS+10 functions as a c-Maf-dependent *Rorc* enhancer in γδ T cells we cloned CNS+10 upstream of a minimal promoter (minP) driving a luciferase reporter, and

assayed activity in wild-type and *Maf*$^{fl/fl}$*Il7r*^{Cre} CD45RB^{lo} γδ T cells. CNS+10 induced a 13-fold increase in activity over that of minP in wild-type cells, that was significantly attenuated in *Maf*$^{fl/fl}$*Il7r*^{Cre} Tγδ17 cells (Fig. 5b). Further, reporter mutation of both MAREs (MAREx2) or individual MAREs diminished CNS+10 activity by 60%, and 20% or 50% respectively (Fig. 5b), implicating CNS+10 as a c-Maf-dependent enhancer. ChIP assay of the histone acetyltransferase p300, which is associated with tissue-specific enhancers[31], showed enriched binding at *Rorc* CNS+10 in CD45RB^{lo} γδ T cells (Fig. 5c), but not T_H17 cells (Fig. 5a). p300 binding at CNS+10 was reduced in E18 *Maf*$^{fl/fl}$*Il7r*^{Cre} CD45RB^{lo} γδ T cells compared with *Maf*$^{+/+}$*Il7r*^{Cre} FT (Fig. 5c). Accordingly, H3K27 acetylation, a product of p300 activity and marker of active enhancers, was also reduced in *Maf*$^{fl/fl}$*Il7r*^{Cre} CD45RB^{lo} γδ T cells at CNS+10 and at the *Rorc(t)* promoter (Fig. 5c). Thus, c-Maf was required for establishing an active regulatory status at the *Rorc* locus in γδ T cells.

To further explore *Rorc* regulation, we evaluated CNS+10 for conserved binding elements and identified TCF1 and RORγt consensus sites (Supplementary Fig. 5). ChIP analysis detected the enrichment of RORγt at *Rorc* CNS+10 in CD45RB^{lo} γδ T cells (Fig. 5d), suggesting RORγt can maintain its own expression. Conversely, TCF1 negatively regulates *Rorc*[12]. Notably, TCF1 also bound CNS+10 in CD45RB^{lo} γδ T cells, and occupancy was elevated in *Maf*$^{fl/fl}$*Il7r*^{Cre} compared to *Maf*$^{+/+}$*Il7r*^{Cre} (Fig. 5d), indicating that c-Maf limits binding of TCF1 to *Rorc*. This effect was specific, as a similar binding enhancement was not observed at *Lef1* (CNS-4kb, Fig. 5d). Moreover, the MARE and TCF1 consensus sites in CNS+10 were in close proximity (Supplementary Fig. 5) and mutation of the TCF1 site enhanced luciferase reporter activity in CD45RB^{lo} γδ T cells compared to wild-type CNS +10 (Fig. 5b). These results suggest that c-Maf can regulate *Rorc* expression by both supporting activating locus modifications and possibly by counteracting the accessibility of TCF1, a negative regulator of type 17 differentiation.

c-Maf is required for type 17 programming in γδ T cells

To uncover c-Maf targets influencing Tγδ17 cell differentiation we performed RNA-sequencing (RNA-Seq) and differential expression analysis in CD25^{-} CD27^{-} γδ T cells from *Maf*$^{fl/fl}$*Il7r*^{Cre} and *Maf*$^{+/+}$*Il7r*^{Cre} E18 FT. This subset is encompassed in the CD45RB^{lo} Tγδ17 population, and present in *Maf*$^{fl/fl}$*Il7r*^{Cre} FT (Supplementary Fig. 6a). Of the significantly differential genes, 70% were downregulated in *Maf*$^{fl/fl}$*Il7r*^{Cre} compared to *Maf*$^{+/+}$*Il7r*^{Cre}. The expression of the core Tγδ17 regulators *Rorc* and *Blk* was severely diminished (Fig. 6a), while expression of other T_H17 cell-associated signature genes, including *Il17a, Il17f, Il23r, Il1r1* and *Ccr6,* was completely abrogated in *Maf*$^{fl/fl}$*Il7r*^{Cre} γδ thymocytes (Supplementary Fig. 6b). Gene set enrichment analysis indicated that the most highly downregulated genes were significantly enriched in top-ranking T_H17 cell network target genes[20] (Supplementary Fig. 6c, d). Thus, c-Maf is a dominant activator of the type 17 program in γδ T cells.

Aside from *Rorc,* the expression of other positive regulators of Tγδ17 cells, namely *Sox4*[12], *Sox13*[12], *Tcf12*[15], *Hes1*[13], *Relb*[32], *Bcl11b*[33] and *Zbtb16*[16], was not significantly altered in *Maf*$^{fl/fl}$*Il7r*^{Cre} CD25^{-}CD27^{-} γδ thymocytes (Fig. 6b). shRNA-mediated knockdown of *Sox13* in fetal liver progenitors prevented c-Maf protein upregulation at the CD45RB^{lo} stage

in OP9-DL1 culture, although *Maf* transcripts were unaltered (Supplementary Fig. 6e), suggesting indirect regulation of c-Maf downstream of Sox13. Unlike positive regulators, expression of Tγδ17 cell negative regulators *Lef1*[12] and *Tcf7* was significantly elevated in *Maf*$^{fl/fl}$*Il7r*^{Cre} cells (Fig. 6b), indicating that c-Maf restricts activators of the Tγδ1 program. This antagonism supports a role for c-Maf as a Tγδ17 commitment factor.

c-Maf and RORγt collaborate in Tγδ17 programming

To determine the mechanism of c-Maf-mediated gene regulation during Tγδ17 lineage commitment, we used ATAC-seq to evaluate changes in chromatin accessibility in immature CD24^{+}CD45RB^{lo} γδ thymocytes from *Maf*$^{fl/fl}$*Il7r*^{Cre} versus *Maf*$^{+/+}$ *Il7r*^{Cre} E18 FT. Consistent with a discrete role for c-Maf in effector programming, only 4% of ATAC regions were differentially accessible (DA) in *Maf*$^{fl/fl}$*Il7r*^{Cre} (Fig. 6c), most displaying reduced accessibility. This included *Rorc, Blk, Il17a, Il17f, Il1r1, Il23r* and *Ccr6* (Fig. 6c). Specifically, we observed significantly diminished chromatin accessibility in the promoter, CNS+10 enhancer, and CNS-1.5 of *Rorc(t)*; and in the MARE-associated CNS of *Il17a* and *Blk* in absence of c-Maf (Fig. 6d). Moreover, 40% of the loci differentially-expressed in *Maf*$^{fl/fl}$*Il7r*^{Cre} γδ thymocytes harbored at least 1 DA region within 10kb of the TSS (versus 8.5% of non-dependent loci, p-value=8×10^{-21} Fisher's exact test), suggesting that c-Maf-dependent changes in chromatin accessibility contribute to gene expression at a substantial portion of loci associated with Tγδ17 effector acquisition.

We next explored whether c-Maf directly regulates accessibility. D*e novo* motif analysis identified consensus sites for RORγt and Maf as the top two most significantly enriched motifs among c-Maf-dependent DA regions in immature Tγδ17 cells (Fig. 6c, Supplementary Fig. 6f). Notably, although MAREs were present in a larger proportion of DA regions than RORE, the RORE motif was significantly more enriched in DA relative to non-DA regions (Supplementary Fig. 6g). As such, a substantial fraction of potential RORγt binding sites in active genomic regions were differentially accessible in the absence of c-Maf. Additionally, RORE-containing regions showed the greatest change in chromatin accessibility among c-Maf-dependent DA peaks (Supplementary Fig. 6h). Thus, c-Maf regulated chromatin accessibility during Tγδ17 commitment, with a potential dominant contribution of its direct target RORγt.

To evaluate whether c-Maf-dependent Tγδ17 programming was mediated by RORγt, we performed differential expression analysis for CD25^{-}CD27^{-} γδ thymocytes from *Rorc(t)*$^{+/+}$ versus RORγt-deficient *Rorc(t)*$^{GFP/GFP}$ E18 FT (Supplementary Fig. 6i). Comparing RORγt- and c-Maf-dependent transcriptomes revealed a high correlation in the regulation of gene expression, particularly in the activation of type 17-associated genes (e.g. *Il17a, Il23r, Il1r1, Ccr6, Gpr183*; Fig. 6e), consistent with c-Maf functioning upstream of *Rorc*. Nevertheless, *Rorc(t)*$^{GFP/GFP}$ fetal γδ thymocytes retained some IL-17A expression (Supplementary Fig. 6j), as reported[13], suggesting direct type 17 regulation by c-Maf. Indeed, both c-Maf and RORγt showed enriched occupancy at *Il17a* CNS-5 in E18 CD45RB^{lo} γδ thymocytes (Fig. 6f), a region that displayed c-Maf-dependent accessibility and enhancer activity in luciferase reporter assay in CD45RB^{lo} Tγδ17 cells (Fig. 6d, Supplementary Fig. 6k). Differential expression analysis also revealed c-Maf-regulated loci

that were independent of RORγt (Fig. 6e), including *Blk*[29], *Syk*[34] and *Lef1*[12]. The conserved MARE in *Blk* CNS+39 was selectively bound by c-Maf in E18 CD45RB^{lo} γδ thymocytes, but not control DN3 cells (Fig. 6g). Additionally, *Blk* CNS+39 displayed c-Maf-dependent accessibility (Fig. 6d), and enhancer reporter activity in CD45RB^{lo} Tγδ17 cells (Supplementary Fig. 6k), implicating *Blk* as a direct c-Maf target. c-Maf also bound to a conserved MARE within the *Tcf7* locus (CNS+16) (Fig. 6g). When cloned upstream of the *Il17a* CNS-5 enhancer in a minimal promoter-driven luciferase construct, *Tcf7* CNS+16 diminished the reporter activity in CD45RB^{lo} γδ T cells (Supplementary Fig. 6k), displaying silencer function. This implies c-Maf may directly attenuate *Tcf7* expression. Therefore, c-Maf directed the Tγδ17 effector programming through RORγt-dependent and –independent regulation of gene expression.

TCR signal strength tunes c-Maf levels during γδ diversification

Next, we investigated signals regulating c-Maf expression in developing fetal γδ thymocytes. Consistent with the idea that strong TCR signals promote the differentiation of Tγδ1 over Tγδ17 cells[9, 11], Vγ3^{+} DETC, which depend on strong ligand-mediated TCR signals[10], lacked high expression of c-Maf compared to Vγ3^{-} γδ thymocytes (Fig. 7a). Additionally, given the positive correlation between surface CD5 levels and TCR signal strength[35], we observed significantly lower CD5 expression on c-Maf^{hi} as compared to c-Maf$^{lo/-}$ E18 γδ thymocytes (Fig. 7b), indicating that c-Maf expression was associated with γδ-selection mediated by relatively weak γδTCR signals.

To directly access whether γδTCR signal strength regulates c-Maf expression, γδ T cell differentiation was induced in developmentally arrested, culture-derived *Rag1*$^{-/-}$ DN T cell precursors via transduction with distinct γδTCR chains derived from the KN6[36], DTN40[37] and C1.21[38] hybridomas, which elicit strong, intermediate and weak signals, respectively[38]. CD5 expression levels confirmed this range for γδTCR-transduced *Rag1*$^{-/-}$ DN2 cells following OP9-DL1 cell culture (Fig. 7c). Notably, we observed an inverse relationship between γδTCR signal strength and both the expression of c-Maf protein and the frequency of c-Maf^{+} γδ T cells (Fig. 7c). In individual cultures of γδTCR-transduced cells, c-Maf^{hi} cells were exclusive to CD5^{lo} populations. Moreover, stronger KN6 TCR signals enhanced production of Tγδ1-associated CD45RB^{hi} cells, whereas weaker C1.21 signals increased generation of CD45RB^{lo}RORγt^{+} Tγδ17 cells (Fig. 7c). Similar results were obtained in γδTCR-transduced *Rag1*$^{-/-}$ total FT DN cells differentiated in fetal thymic organ cultures (Supplementary Fig. 7a). While Tγδ17 cells derive mainly from DN2 cells[33], *Rag1*$^{-/-}$ DN3 cells retained the potential to generate RORγt^{+} γδ T cells in culture, when provided with a weak γδTCR signal (Supplementary Fig. 7b). Thus, weak γδTCR signals were most permissive to high expression of c-Maf and Tγδ17 differentiation.

To interrogate individual TCR signaling pathways in the regulation of c-Maf protein expression, culture-derived DN3 cells were transduced with constitutively active kinase mutants and differentiated in OP9-DL1 cultures. Lck^{F505}, which recapitulates TCR-proximal signaling[39], mimicked the effects of strong TCR signals (Fig. 7c), resulting in a marked reduction in c-Maf expression and in the frequency of CD45RB^{lo}c-Maf^{+}RORγt^{+} γδ T cells compared to the control vector (Fig. 7d). Lck activates downstream PKC and Ras-MAPK

kinase cascades. Whereas transduction of a catalytically active PKC marginally effected γδ T cell development (Fig. 7d), active Ras^{V12} resulted in a striking enhancement in c-Maf protein and a near-complete conversion to a $CD45RB^{lo}$c-$Maf^{+}ROR\gamma t^{+}$ γδ T cell phenotype (Fig. 7d). Because Ras is also activated by growth factor and cytokine receptors, the opposing effects of Lck^{F505} and Ras^{V12} suggest strong TCR signals limit c-Maf, whereas non-TCR MAPK-independent Ras signals promote c-Maf expression. Thus, TCR signal quality and intensity permit for graded levels of c-Maf protein, allowing c-Maf to function as a rheostat controlling effector γδ T cell generation.

Discussion

Here we identified c-Maf as an essential regulator of Tγδ17 differentiation, required for the induction and maintenance of $ROR\gamma t^{+}$ γδ T cells. c-Maf directly activated *Rorc* and key genes in the type 17 γδ effector program (*Il17a, Blk*), while antagonizing negative regulators of Tγδ17 differentiation such as TCF1 (*Tcf7*) and *Lef1* that promote the alternative Tγδ1 fate. Globally, c-Maf was required to establish a Tγδ17 accessibility landscape, with particular importance at a subset of defining effector loci and enhancer elements. c-Maf expression was tuned by γδTCR signal strength, providing a mechanism for how weak signals are translated into Tγδ17 effector specialization. Taken together, our findings define c-Maf as a core node in the Tγδ17 network and provide novel insights into molecular mechanisms of γδ T cell effector fate acquisition.

c-Maf is selectively required for type 17 specialization in γδ T cells. Indeed, c-Maf was not essential for *Rorc* expression in DP, ILC or T_H17 cells *in vivo.* Although c-Maf contributes to *Rorc* expression in T_H17 cells, this occurs indirectly via repression of IL-2[40]. The distinct occupancy patterns of c-Maf in *Rorc* CNS in γδ T cells compared to T_H17 cells explain the unique lineage-specific functions of c-Maf. Globally, c-Maf as an activator in Tγδ17 cells *versus* repressor in T_H17 cells[20]. Context-dependent c-Maf activity may be governed by differences in epigenetic programming, as c-Maf contributes to the establishment of an effector-associated active regulatory landscape in Tγδ17 cells, but not in $CD4^{+}$ T cells where differential accessibility implicates Runx factors in chromatin remodeling[40]. Moreover, in T_H17 cells, pioneering and *Rorc* activation are served by IRF4, BATF and STAT3[20, 41], which are dispensable for Tγδ17[13, 42]. Thus, c-Maf has distinct modes of gene regulation in γδ T cells *versus* $CD4^{+}$ helper T cells.

We define a trajectory for Tγδ17 effector acquisition from post γδ-selected $\gamma\delta TCR^{int}CD45RB^{int}$c-$Maf^{lo}$ cells to specialized mature $CD45RB^{lo/-}CD24^{-}ROR\gamma t^{+}$c-$Maf^{hi}$ cells. The absolute c-Maf-dependency of this process uncouples effector programming from upstream γδ-selection events, revealing a Tγδ17 specialization checkpoint at the immature $CD45RB^{lo/-}CD24^{+}$ γδ T cell stage. This is consistent with the identification of $CD45RB^{-}CD44^{-}$ γδ fetal thymocytes as precursors for Tγδ17 cells[11]. The block also provides genetic support for a model in which effector programming is molecularly distinct from γδ-selection[43]. We defined a second checkpoint at the $CD45RB^{lo}ROR\gamma t^{lo}$ stage whereby survival and Tγδ17 identity required continued c-Maf expression. Thus, Tγδ17 effector commitment spans several c-Maf-dependent developmental stages. This may account for the

temporal delay in the capacity for full effector cytokine expression following the expression of RORγt in γδ thymocytes[11].

Discrete regulators control the specialization of distinct subsets of Tγδ17 cells defined by developmental stage, anatomical location, or Vγ usage[12, 15]. We identify c-Maf as a universal, non-redundant regulator of type 17 programming required for the generation and maintenance of all subsets of Tγδ17 cells. This implicates two tiers of regulators in specialization: TCR-independent specification factors (e.g. Sox13) that perceive environmental signals to establish discrete Tγδ17 subsets, and commitment factors (e.g. c-Maf) that impart or reinforce effector identity. Thus, c-Maf-dependence represents a unifying feature of Tγδ17 cell development.

c-Maf integrates various nodes in the Tγδ17 regulatory network. c-Maf and RORγt collaborate in regulation of *Il17a* in CD45RB^{lo} γδ thymocytes. c-Maf cooperates with Sox4 and Sox13 to directly activate *Rorc, Blk* and *Il17a* expression[12]. The proximity of MARE and HMG box consensus sites in *Rorc* CNS+10 suggests physical and functional cooperativity between c-Maf and Sox factors in γδ thymocytes, as described in other cell types[44, 45]. Such collaboration could integrate parallel regulatory pathways of discrete Tγδ17 subset specification by Sox and universal type 17 effector commitment by c-Maf. We found the negative regulator TCF1 also occupied *Rorc* CNS+10. As Sox and TCF factors bind related HMG box recognition elements, c-Maf-Sox cooperativity via a composite MARE-HMG box consensus site may account for c-Maf antagonism of TCF1 occupancy. A similar lineage promotion and antagonism relationship for c-Maf and TCF1 occurs in Th17 cells[46], implying a conserved c-Maf-HMG box regulatory axis in type 17 specialization.

How does analog γδTCR stimulation translate into distinct effector fate outcomes? Differences in γδTCR signal strength result in graded expression of c-Maf, linking TCR signals to Tγδ17 effector programming. Signaling modalities compatible with the induction of c-Maf by weak γδTCR have been proposed[47]. γδTCR signals may also provide initial licensing—via *Maf* accessibility or secondary targets—required for c-Maf induction by environmental signals. In this regard, Notch and TGF-β are activators of c-Maf in CD4$^+$ T cells[19, 48]. Moreover, TGF-β activates Ras signaling[49], which potently promotes c-Maf expression in γδ T cells. This suggests that while strong activation of the MAPK-ERK-Egr-Id3 pathway promotes Tγδ1 fate[10, 47], MAPK-independent Ras signals promote c-Maf and Tγδ17 fate. The finding that PI3K, a Ras target, is selectively essential for Tγδ17 subset differentiation[34] supports this view. Thus, c-Maf may integrate TCR and environmental inputs, permitting appropriate effector acquisition. How the resulting graded c-Maf expression is resolved into Tγδ17 fate remains to be determined. In this regard, a graded rheostat mechanism converts to a digital on-off switch when activators and repressors compete for the same regulatory element[50]. It is interesting to speculate that such interactions between c-Maf and TCF1—as is the case at *Rorc* CNS+10—determine γδ T cell identity. Future work deciphering the extrinsic factors and signaling pathways that regulate c-Maf will shed light on the intricate process of innate-like functional programming in the thymus.

Online Methods

Mice

Mice were used in accordance with the Duke University Institutional Animal Care and Use Committee guidelines and housed under specific pathogen-free conditions. Mice bearing a floxed allele of *Maf* (*Maf*$^{f/f}$) were obtained from C. Birchmeier (Max-Delbrück Center for Molecular Medicine, Germany)[27], and backcrossed to C57BL/6 for at least 5 generations. *Il7r*^{Cre} mice expressing Cre from the *Il7r* locus were obtained from H.R. Rodewald (German Cancer Research Center, Germany)[26]. *Rorc*-Cre mice (Stock 022791, Jackson), C57Bl/6 (Taconic), *Rorc(t)*^{GFP} mice (Stock 007572, Jackson), *Rag1*-deficient (Stock 002216, Jackson), and C57BL/6 CD45.1 congenic (Stock 002014, Jackson) were bred in our facility. Timed pregnant females were generated using the Whitten effect, and CD-1 pregnant females were purchased from Charles River (Stock 022). For determination of embryonic ages, noon on the day of the post-coital plug was considered to be E0.5. Adult mice between 8 and 12 weeks of age were used in experiments. Mutants were compared to littermate controls. Adult *Maf*$^{fl/fl}$ Cre^{+} genotype mice harboring cells that escaped *Maf* deletion, based on positive intracellular c-Maf protein staining by flow cytometry, were excluded from analyses.

Isolation of hematopoietic cells from adult and fetal tissues

Cell isolation from the thymus, spleen, inguinal lymph nodes, skin, and small intestine lamina propria (SILP) was performed as previously described[51], with the modification that HBSS used for digestion and washing of intestine was supplemented with 10% FBS and 10mM HEPES. For cell isolation from the reproductive tract, the cervix, uterine horn, and vagina were combined and processed similar to the SILP, except that the digestion time was extended to 60 minutes. For mouse fetal tissues, E15–18 fetal thymii and E14–15 fetal liver (FL) were harvested and single-cell suspensions were generated by disruption through a 40 μm nylon mesh using a syringe plunger. CD24$^{low/-}$ FL hematopoietic progenitor cells (HPC) were enriched by antibody-and complement-mediated lysis. Here, cell suspensions from up to 30 FL were incubated in a total of 10 mL of complete medium containing 2.5 μg/mL of purified anti-CD24 (J11d, BD Biosciences) and a 1:10 dilution of Low-tox rabbit complement (Cedarlane) for 30 min at 37°C. Viable HPC were recovered by density gradient centrifugation over Lympholyte-M (Cedarlane), and washed once in complete medium prior to culture or transduction.

T cell stimulation and flow cytometry

To analyze cytokine production, cells were incubated with phorbol 12-myristate 13-acetate (PMA, 100 ng/ml; Sigma), ionomycin (375 ng/ml; Sigma), and IL-23 (10 ng/mL, eBioscience) in the presence of GolgiStop (BD) for 4 h at 37°C in complete RPMI (10% FBS, 10 U/mL penicillin, 10 μg/mL streptomycin, 2 mM glutamine, 10 mM HEPES, 1 mM sodium pyruvate, 50 μg/mL gentamycin, and 55 μM β-mercaptoethanol). Cell surface staining, fixation, and intracellular staining for cytokines or transcription factors was performed as described[51]. AnnexinV binding (Apoptosis Detection kit; eBioscience) was performed prior to fixation according to the manufacture's suggested protocol. For live cell sorting, cells were surface stained in Ca^{2+}/Mg^{2+}-free PBS containing 0.5% BSA and 2 mM

EDTA for 30 min on ice, washed once, and resupended in staining buffer for sorting using MoFlo Astrios or XDP cell sorters (Beckman Coulter). In all instances, dead cells were excluded by including a fixable viability dye (eBiosciences) during cell surface staining. Antibodies for staining were purchased from eBiosciences (CD117, CD11b, CD11c, CD19, CD3ε, CD4, CD24, CD25, CD27, CD44, CD45, CD45.1, CD45RB, CD62L, CD73, CD8α, c-Maf, Eomes, γδTCR, GFP, Gr-1, IFNγ, IL-17A, NK1.1, RORγt, rabbit IgG, T-bet, TCRβ, Ter119, Vγ2); BD (CCR6, H2Db); Biolegend (CD5, CD127, Vγ1.1, Vγ3), or Cell Signaling Technologies (TCF1). All data were acquired on a FACSCanto II (BD Biosciences) and analyzed using FlowJo software (Tree Star). All analyses are pre-gated for single, live cells, except for AnnexinV binding analysis.

Cell Culture

OP9-DL1 cells (provided by J.C. Zuñiga-Pflücker, Sunnybrook Research Institute, Toronto) were maintained in IMDM media (Sigma) supplemented with 10% FBS, penicillin (10 U/mL), streptomycin (10 μg/mL), gentamicin (50 μg/mL), and β-mercaptoethanol (55 μM) (complete IMDM). To generate DN2 and DN3 cells for transduction, 750 thousand B6 or CD-1 FL HPC were cultured in complete IMDM with confluent monolayers of OP9-DL1 cells in a 10cm plate in the presence of 1ng/mL IL-7 and 5ng/mL Flt3L (eBioscience) for 5 days. For γδ T cell differentiation, progenitor cells were sort-purified from pooled FT on the indicated date of gestation or from post transduction FL/OP9DL1 cultures. FT progenitor populations included DN2 ($CD4^-$ $CD8^-$ $Ter119^-$ $NK1.1^-$ $CD3\varepsilon^-$ $\gamma\delta TCR^-$ $CD117^{hi}$ $CD25^+$), DN3 ($CD4^-$ $CD8^-$ $Ter119^-$ $NK1.1^-$ $CD3\varepsilon^-$ $\gamma\delta TCR^-$ $CD117^{lo}$ $CD25^+$), and $CD45RB^{int}$ γδ T cells ($CD4^-$ $CD8^-$ $Ter119^-$ $CD3\varepsilon^+$ $\gamma\delta TCR^{lo}$ $CD45RB^{int}$). FL/OP9-DL1 populations included DN2 ($CD4^-$ $CD8^-$ $CD3\varepsilon^-$ $\gamma\delta TCR^-$ $CD44^+$ $CD25^+$) and DN3 cells ($CD4^-$ $CD8^-$ $CD3\varepsilon^-$ $\gamma\delta TCR^-$ $CD44^-$ $CD25^+$). Sorted populations were cultured with monolayers of OP9-DL1 cells in 48 well plates of complete IMDM in the presence of 1ng/mL IL-7 (eBioscience) as follows: 5,000 DN2, 10,000 DN3, 10,000 $CD45RB^{int}$ γδ T cells per well.

Retroviral Gene Transfer

Retroviral constructs were generated by cloning cDNA for c-Maf, RORγt, and Blk into MSCV-Thy1.1 5' of the internal ribosomal entry site, allowing bicistronic expression with cell surface Thy1.1. Retroviral constructs for expression of active kinases and TCRγδ chains were generously provided by J.C. Zuñiga-Pflücker (University of Toronto). This includes, constructs expressing LckF505, PKCαCAT, or RasV12 with GFP in MSCV-based MigR[52]; and KN6, DTN40 or C1.21 hybridoma cDNAs for TCRγ with GFP in MigR and TCRδ with YFP in MIY[38]. Retroviral supernatants were generated by transfection of retroviral constructs into the Plat-E producer cell line[53] using Lipofectamine 2000 reagent (ThermoFisher scientific), and collection of after 48h. In the case of γδTCR chains, equal amounts of MigR-TCRγ and MIY-TCRδ constructs were co-transfected to permit co-transduction. Lentiviral constructs were generated by annealing of oligos for short hairpins targeting either Sox13 test (hairpin 5'-CCAGCAGGTTAACATGCCTTA-CTCGAG-TAAGGCATGTTAACCTGCTGG-3') or luciferase control (hairpin 5'-CGCTGAGTACTTCGAAATGTC-CTCGAG-GACATTTCGAAGTACTCAGCG-3') genes and ligating into the pLKO.3-Thy1.1 vector (provided by C. Benoist & D Mathis via

Addgene plasmid #14749) for U6-mediated shRNA expression and Thy1.1 reporter. Lentiviral supernatants were produced by transfection of pLKO.3-Thy1.1-shSox13 or pLKO.3-Thy1.1-shLuc vectors with pCMV-Δ8.91 (*gag, pol, rev*) and p-VSVG envelope expression plasmids into the 293FT producer cell line using Lipofectamine 2000 reagent and collection of after 48h.

For gene transfer, DN-enriched thymocytes were prepared from single cell suspensions of E15-E17 FT by depletion of $CD4^+$ cells using magnetic-activated cell sorting (MACS, Miltenyi) following the manufacture's protocol. Alternatively, FL-derived DN cells were harvested on day 5 of coculture with OP9-DL1 cells. In all cases, single cell suspensions of DN T cell precursors were resuspended in 0.45μ-filtered viral supernatant containing 6.7μg/mL of hexadimethrine bromide (Sigma-Aldrich), transferred to 48, 24, or 12 well plates at $\leq 0.5 \times 10^6$ cells/cm^2, and spun at 2400 rpm for 2h at 30°C. Cells were placed in OP9-DL1 cultures with 1ng/mL IL-7 and 5ng/mL Flt3L overnight sorted for transduced populations of interests (i.e. $Thy1.1^+$ or YPF^+ GFP^+ double-expressing). In the case of introduction of TCRγ and TCRδ chains into *Rag1*$^{-/-}$ fetal thymocytes, total DN cells were transduced and immediately transferred into FTOC.

Fetal thymic organ culture (FTOC)

Fetal organ cultures were performed in high glucose DMEM (Gibco-ThermoFisher) supplemented with 15% FBS, penicillin (10 U/mL), streptomycin (10 μg/mL), gentamicin (50 μg/mL), and β-mercaptoethanol (55 μM) (FTOC media). Reconstitution FTOCs were performed using supportive rafts composed of gelfoam sponges and Millipore filters as described[54]. Briefly, $CD45.1^+$ FT recipient lobes were isolated from E14.5 embryos and treated with 1.35 mM deoxyguanosine for 5 days and rested for 2 days to deplete endogenous thymocytes. Depleted lobe pairs were placed in overnight hanging drop culture with 5,000 transduced *Rag1*$^{-/-}$ fetal thymocytes and moved to raft cultures the next day for differentiation. For reaggregate fetal thymic organ cultures (RTOC), depleted FT lobes were washed twice in PBS and digested in 600μL of 0.05% Trypsin/EDTA (Gibco-ThermoFisher) for 30 minutes at 37°C. Digest was quenched with 600μL of FTOC media and a single cell suspension was generated by repeated pipetting until the majority of FT were disrupted. The FT suspension was filtered, spun, and resuspended in FTOC media. To form RTOC, 700,000 stromal cells and between 1,000 and 10,000 γδ T cell progenitor cells were combined and spun down together. The resulting pellet was drawn up in a pipette tip and deposited directly onto the raft filter for differentiation. *Rag1*$^{-/-}$ FT stroma was used for RTOCs reconsituted with mixtures of wild-type ($CD45.1^+$) and *Maf*-deficient ($CD45.2^+$) progenitors. Fetal organ cultures were performed in the presence of 1ng/mL IL-7 (eBioscience).

Immunoblotting

Western blots were performed as previously described[51]. Transduced $CD4^-$ $CD8^-$ cells were sorted for Thy1.1 expression on day 10 of FL HPC/OP9-DL1 culture and 300 thousand cells were resuspended in RIPA buffer to make cell lysates. Anti-Sox13 (1:500, Abcam, ab96776) was used to detect Sox13 knockdown and normalized to an anti-actin (1:400, BD, 612656) loading control with ImageJ.

Luciferase assay

Select MARE-containing *cis* regions within the *Rorc, Blk,* and *Il17a* loci were assessed by dual luciferase reporter assay for enhancer activity by cloning the sequences upstream of a minimal promoter driving a luciferase gene (pGL4.21). Silencer activity for *Tcf7* CNS+16 was determined by cloning the region upstream of the *Il17a* CNS-5 enhancer in the pGL4.21 minimal promoter construct. Site-directed mutagenesis of *Rorc* CNS+10 was performed by non-overlapping primer amplification of pGL4minP-*Rorc* CNS+10 followed by template digestion with DpnI (NEB), and blunt ligation of the resulting mutated amplicon. Fetal liver derived HPC were differentiated in OP9-DL1 cultures supplemented with 5ng/mL Flt3L and 1ng/mL IL-7 for the first 5 days and for 1ng/mL IL-7 alone thereafter. CD4- CD8- CD45RB^{lo} CD3ε^{+} TCRγδ^{+} γδ T cells were sort purified on day 11 of culture for nucleofection using a Lonza 4D-Nucleofector with solution P3 for primary cells and pulse code DN100 according to the manufacturer's protocol. In brief, approximately 360–400 thousand cells were nucleofected with 0.17μg of pCMV-RL and 0.83μg of test or empty pGL4minP construct. Pre-warmed media was added to cells prior to transfer to 96 well plates for culture in growth media containing 1ng/mL IL-7. Cells were harvested after 24h for assay using the Dual Luciferase Reporter Assay System (Promega E1910). For each sample, firefly luciferase measurements were normalized to renila luciferase values and data is presented as fold change relative to empty pGL4minP or to wild-type *Rorc* CNS+10-pGL4minP, as appropriate.

RNA preparation, sequencing, and RNA-seq differential expression analysis

RNA was extracted from 10–90 thousand CD27^{-} CD25^{-} TCRγδ^{+} CD3ε^{+} E17–18 fetal thymocytes cells using Trizol (Invitrogen), with the aqueous phase subjected to RNA purification using the RNeasy Plus Micro Kit (Qiagen). To obtain sufficient material for sequencing, samples from multiple fetuses were pooled prior to RNA purification. Library preparation was performed by the Duke Sequencing and Genomic Technologies Shared Resource facility using the Clontech SMARTer v3/v4 ultra-low input RNA-seq kit (Takara Biosciences). Libraries were subsequently sequenced to 50bp in single-end mode on either an Illumina HiSeq 2000/2500 (for 2 replicate c-Maf samples) or HiSeq 4000 (for 4 replicate *Rorc(t)*^{GFP} samples) to a depth of 30–50 million reads per sample.

All RNA-seq samples were first validated for consistent quality using FastQC v0.11.7 (Babraham Institute). Raw reads were trimmed to remove adapters and bases with Q < 20 using Trim Galore! with Cutadapt v0.4.4_dev (Babraham Institute). Adapter- and quality-trimmed reads were subsequently aligned to the GRCm38 mouse genome (GENCODE; mm10) using STAR v2.6.0a[55] allowing for no novel splice junctions (--alignSJoverhangMin 500) and keeping only uniquely-mapped reads (--outFilterMultimapNmax 1).

Aligned reads were assigned to genes in the GENCODE GRCm38 comprehensive gene annotation (ver. M17) using featureCounts (v1.6.2) with default settings[56]. Differential expression analysis was performed using edgeR (ver 3.22.3)[57] running on R (ver 3.5.0). Briefly, raw counts were imported and filtered to remove genes with low or no expression (i.e. having less than 2 counts-per-million in all experimental groups). Filtered counts were then normalized for library size using calcNormFactors(), followed by estimation of

common, trended, and tagwise dispersion using estimateDisp(). Differential expression was calculated using the exactTest method, with genes having a Benjamini-Hochberg false discovery rate (FDR) less than 0.05 being considered significant (unless otherwise indicated). For estimating transcript abundance, reads per kilobase million (RPKM) was determined from normalized read counts using the edgeR rpkm() function. Data were visualized using ggplot2 (ver. 3.0.0).

Assay for Transposase-Accessible Chromatin (ATAC) Sample Preparation and Sequencing

15 to 17 thousand $CD4^-$ $CD8^-$ $TCR\gamma\delta^+$ $CD3\varepsilon^+$ $CD24^+$ $CD45RB^{lo}$ thymocytes were sort purified from pooled E17-E18 $Maf^{+/+}$ $Il7r^{Cre}$ and $Maf^{fl/fl}$ $Il7r^{Cre}$ fetuses. Omni-ATAC[58] was performed with slight modifications on two biological replicates per genotype using Tn5 transposase from the Nextera DNA Library Prep Kit (FC-121–1030). The transposition reaction was scaled according to cell number to be proportional to a 50ul reaction for 50,000 cells (~17,000 cells in a 17ul reaction). After the transposition reaction, DNA was purified with the Qiagen MinElute Kit (28204). For amplification, samples underwent 4–6 additional PCR cycles based on the qPCR amplification curves after the 5 pre-amplification cycles (9–11 total cycles). For cleanup and size-selection of libraries, AMPure beads (Agilent A63880) were used at 0.5X to remove >1,000kb fragments followed by 1.8X to remove primer dimers. ATAC libraries were sequenced at the Duke Sequencing and Genomic Technologies Shared Resource facility on an Illumina NextSeq 500 using 42 bp paired-end reads to a depth of 75–100 million reads per sample.

ATAC-seq Preprocessing and Alignment

As with RNA-seq, data quality was first validated using FastQC, followed by adapter and quality trimming (Q > 20) using Trim Galore. Trimmed reads were aligned to the GRCm38 genome using Bowtie2 (ver. 2.3.4.1) with '--very-sensitive' settings[59]. Reads mapping to the ENCODE mm10 blacklisted regions (www.encodeproject.org; regions with anomalous high signal across multiple genomic assays and cell types) were removed using bedtools2 intersect (ver. 2.27.1)[60]. Properly paired reads were then filtered to exclude presumed PCR duplicates using Picard MarkDuplicates (ver. 2.18.9; http://broadinstitute.github.io/picard/). Fragment size distribution were visualized using deeptools (ver. 3.1.2)[61] which showed the majority of fragments were mononucleosomal or smaller. To eliminate the contribution of larger, polynucleosomal reads from our analysis, we excluded fragments larger than 175 bp using samtools 1.8[62] and a custom perl-based filter. Size filtered reads were then used to generate rpkm-normalized bigWig files for visualization using deeptools bamCoverage. Because our samples were comprised of pooled, mixed-gender fetal tissues, we excluded X and Y chromosomes during bigWig normalization to eliminate the influence of sample-to-sample variation in sex composition.

Differential ATAC Analysis

Reads processed as above were used to call peaks for each sample individually using MACS2[63] (ver. 2.1.1) with options 'callpeak –nomodel -f BAMPE -q 0.1'. Sample-specific peaksets were then combined into a master peakset using bedtools merge, which was then used for all downstream analyses. The number of reads in each sample mapping to each peak was calculated using featureCounts, with duplicate reads excluded (--ignoreDup) and

reads overlapping multiple features assigned to the feature with the largest overlap (--largestOverlap). Count data was then imported into R and preprocessed to remove all reads mapping to X and Y chromosomes (due to potential sex imbalance in pooled samples) as well as mitochondrial DNA. Filtered counts were then processed using edgeR, removing any peaks having less than 2 counts per million in more than 2 samples. Counts were normalized for library size, common, trended, and tagwise dispersions were calculated, and differential expression analysis performed using the exactTest method with prior count increased to 1 to reduce overestimation of log fold-change values for low-abundance differential peaks. Regions having a Benjamini-Hochberg FDR below 0.05 were considered to have significantly different accessibility between groups. IGV ver. 2.4.14 (Broad Institute) was for visualization of ATAC- and ChIP-seq tracks.

ChIP-seq Analysis

Publicly-available c-Maf, p300, RORγt ChIP-seq data were obtained from GEO (GSE40918)[20] as raw FASTQ files (Ciofani 2012). Data preprocessing and alignment were performed as for ATAC seq (above), except that size analysis and exclusion was not performed. Peaks were called versus input controls using MACS2 with a q-value threshold of 0.05. To generate a high-confidence peakset for use in *de novo* motif identification, we took the intersection of replicates using bedtools (keeping only regions called independently in both replicates).

Motif Enrichment Analysis

To identify transcription factor binding motifs enriched in differential ATAC-seq peaks, we performed both *de* novo and known motif enrichment analysis using HOMER findMotifsGenome.pl (ver. 4.1.0)[64]. Full-length differential ATAC peaks with an FDR < 0.05 were provided as foreground, with non-differential ATAC peaks used background. For *de novo* predictions of c-Maf and RORγt motifs from Th17 cell ChIP-seq data, we used the same method except that HOMER-calculated GC-normalized genomic regions were used as background with high-confidence ChIP-seq peaks as foreground.

Motif Scanning

For visualizing c-Maf and RORγt binding sites as well as determining overlap with ATAC-seq peaks, we used HOMER scanMotifGenomeWide.pl with a p-value of 0.05 to locate putative binding sites across the mm10 genome. As input, the following motifs were provided for both c-Maf and RORγt: (1) The top-scoring *de novo*-predicted motif from ChIP-seq, (2) the related top-scoring *de novo*-predicted motif from differential ATAC-seq, (3 & 4) the first and second-highest scoring *known* motif from the appropriate TF family (ROR or Maf) for ATAC-seq.

ATAC-seq Peak Annotation

We employed several methods to classify and annotate ATAC-seq peaks. To identify peaks associated with c-Maf and/or RORγt motifs and/or ChIP-peak, we used bedtools intersect to identify motifs having direct overlap with predicted motif locations or ChIP-peaks across the genome. To associate peaks with putative target genes, we considered peaks within 10kb up-

or down-stream of the gene body (TSS to TES) of a given gene to be associated with that gene. These associations were made using bedtools window function, with a window size of 10,000 and all *expressed* loci (as determined from c-Maf differential expression analysis) used as input.

Candida albicans infection

C. albicans strain SC5314 was kindly provided by Dr. Joseph Heitman (Duke University). *C. albicans* growth and infection was performed as described[51]. Briefly, 2×10^8 yeast were applied in 50ul PBS to a 2 cm x 2 cm plucked and abraded area of the lower back of mice. Skin was harvested three days post infection to establish infection load. For this, a $1cm^2$ central area was minced in 1 mL of PBS, homogenized, serially diluted, and grown on YPD plates at 30°C for 24 h to determine CFUs.

Chromatin Immunoprecipitation

Total γδ T cells ($CD4^-$ $CD8^-$ $Ter119^-$ $CD3\varepsilon^+$ $\gamma\delta TCR^+$), DN3 cells ($CD4^-$ $CD8^-$ $Ter119^-$ $CD3\varepsilon^-$ $\gamma\delta TCR^-$ $CD117^{-/lo}$ $CD25^+$), and $CD45^{lo}$ γδ T cells ($CD4^-$ $CD8^-$ $Ter119^-$ $CD3\varepsilon^+$ $\gamma\delta TCR^+$ $CD45RB^{lo/-}$) were sort purified from C57BL/6, *Maf*$^{+/+}$ *Il7r*^{Cre}, or *Maf*$^{fl/fl}$ *Il7r*^{Cre} E18 FT, as indicated. For Th17 cells, sort purified naïve CD4 T cells ($CD4^+$ $CD25^-$ $CD62L^+$ $CD44^{lo/-}$) were differentiated for 48h *in vitro* in the presence of 20 ng/mL IL-6 and 0.3 ng/mL TGFβ (eBioscience), as previously described[51]. Depending on the cell population, 50 thousand to 3 million cells were used for ChIP experiments. ChIP was performed as reported[51]. Commercial antibodies used include c-Maf (Bethyl Laboratories, A300–613A), p300 (Santa Cruz Biotech, C-20; sc-585), and H3K27ac (Abcam, ab4729). RORγt antiserum was raised in rabbits against amino-acids 79–301(Covance) and antibody was purified on Protein A-conjugated columns. The TCF1 antiserum was kindly provided by Dr. Hiroshi Kawamoto (Kyoto University, Japan). Test and control regions were amplified within ChIP-enriched and input DNA by qPCR, and data are represented as percent of input. Primer sequences are provided in Supplementary Table 1.

Statistical analysis

Expect for RNA-seq experiments, all statistical analyses were performed using GraphPad Prism 7. For cellular phenotyping and ChIP assay, an unpaired two tailed Student's *t* test was used to establish the significance of the differences observed between two populations of cells. Parametric tests were used when variance between groups was similar, as determined by F-tests; however when variance was significantly different non-parametric tests were performed. In the case of two independent variables, statistical significance was determined by two-way ANOVA with Fisher's least significant difference posttest. Specific statistical tests are indicated in the figure legends. Information summarizing statistical analysis and methods can be found in the accompanying Life Sciences Reporting Summary.

Supplementary Material

Refer to Web version on PubMed Central for supplementary material.

Acknowledgements

We thank C. Birchmeier (Max Delbrück Center for Molecular Medicine, Germany) for providing *Maf* conditional mice; J.C. Zuñiga-Pflücker (University of Toronto) for providing OP9-DL1 cells; H. Kawamoto (Kyoto University, Japan) for providing TCF1 antibody; J. Heitman (Duke University) for providing *C. albicans* strain SC5314; and R. DePooter for critical reading of the manuscript. We acknowledge the expert assistance of N. Martin and L. Martinek with flow cytometry. This work was funded by a Whitehead Scholar Award (to M.C.). J.W. and M.C. were supported by NIH grant R01 GM115474. M.C was supported by a Career Development Award from the Crohn's and Colitis Foundation of America.

References

1. Shibata K, Yamada H, Hara H, Kishihara K & Yoshikai Y Resident Vdelta1+ gammadelta T cells control early infiltration of neutrophils after Escherichia coli infection via IL-17 production. Journal of immunology 178, 4466–4472 (2007).
2. Conti HR et al. Oral-resident natural Th17 cells and gammadelta T cells control opportunistic Candida albicans infections. The Journal of experimental medicine 211, 2075–2084 (2014). [PubMed: 25200028]
3. Papotto PH, Reinhardt A, Prinz I & Silva-Santos B Innately versatile: gammadelta17 T cells in inflammatory and autoimmune diseases. J Autoimmun (2017).
4. Ribot JC et al. CD27 is a thymic determinant of the balance between interferon-gamma- and interleukin 17-producing gammadelta T cell subsets. Nature immunology 10, 427–436 (2009). [PubMed: 19270712]
5. Havran WL & Allison JP Origin of Thy-1+ dendritic epidermal cells of adult mice from fetal thymic precursors. Nature 344, 68–70 (1990). [PubMed: 1968230]
6. Itohara S et al. Homing of a gamma delta thymocyte subset with homogeneous T-cell receptors to mucosal epithelia. Nature 343, 754–757 (1990). [PubMed: 2154700]
7. Xiong N & Raulet DH Development and selection of gammadelta T cells. Immunol Rev 215, 15–31 (2007). [PubMed: 17291276]
8. Haas JD et al. Development of interleukin-17-producing gammadelta T cells is restricted to a functional embryonic wave. Immunity 37, 48–59 (2012). [PubMed: 22770884]
9. Jensen KD et al. Thymic selection determines gammadelta T cell effector fate: antigen-naive cells make interleukin-17 and antigen-experienced cells make interferon gamma. Immunity 29, 90–100 (2008). [PubMed: 18585064]
10. Turchinovich G & Hayday AC Skint-1 identifies a common molecular mechanism for the development of interferon-gamma-secreting versus interleukin-17-secreting gammadelta T cells. Immunity 35, 59–68 (2011). [PubMed: 21737317]
11. Sumaria N, Grandjean CL, Silva-Santos B & Pennington DJ Strong TCRgammadelta Signaling Prohibits Thymic Development of IL-17A-Secreting gammadelta T Cells. Cell Rep 19, 2469–2476 (2017). [PubMed: 28636936]
12. Malhotra N et al. A network of high-mobility group box transcription factors programs innate interleukin-17 production. Immunity 38, 681–693 (2013). [PubMed: 23562159]
13. Shibata K et al. Notch-Hes1 pathway is required for the development of IL-17-producing gammadelta T cells. Blood 118, 586–593 (2011). [PubMed: 21606479]
14. Do JS et al. Cutting edge: spontaneous development of IL-17-producing gamma delta T cells in the thymus occurs via a TGF-beta 1-dependent mechanism. Journal of immunology 184, 1675–1679 (2010).
15. In TSH et al. HEB is required for the specification of fetal IL-17-producing gammadelta T cells. Nature communications 8, 2004 (2017).
16. Lu Y, Cao X, Zhang X & Kovalovsky D PLZF Controls the Development of Fetal-Derived IL-17+Vgamma6+ gammadelta T Cells. Journal of immunology 195, 4273–4281 (2015).
17. Bauquet AT et al. The costimulatory molecule ICOS regulates the expression of c-Maf and IL-21 in the development of follicular T helper cells and TH-17 cells. Nature immunology 10, 167–175 (2009). [PubMed: 19098919]

18. Ho IC, Hodge MR, Rooney JW & Glimcher LH The proto-oncogene c-maf is responsible for tissue-specific expression of interleukin-4. Cell 85, 973–983 (1996). [PubMed: 8674125]
19. Rutz S et al. Transcription factor c-Maf mediates the TGF-beta-dependent suppression of IL-22 production in T(H)17 cells. Nature immunology 12, 1238–1245 (2011). [PubMed: 22001828]
20. Ciofani M et al. A validated regulatory network for th17 cell specification. Cell 151, 289–303 (2012). [PubMed: 23021777]
21. Yu JS et al. Differentiation of IL-17-Producing Invariant Natural Killer T Cells Requires Expression of the Transcription Factor c-Maf. Front Immunol 8, 1399 (2017). [PubMed: 29163480]
22. Wheaton JD, Yeh CH & Ciofani M Cutting Edge: c-Maf Is Required for Regulatory T Cells To Adopt RORgammat(+) and Follicular Phenotypes. Journal of immunology 199, 3931–3936 (2017).
23. Xu M et al. c-MAF-dependent regulatory T cells mediate immunological tolerance to a gut pathobiont. Nature 554, 373–377 (2018). [PubMed: 29414937]
24. Narayan K et al. Intrathymic programming of effector fates in three molecularly distinct gammadelta T cell subtypes. Nature immunology 13, 511–518 (2012). [PubMed: 22473038]
25. Barbee SD et al. Skint-1 is a highly specific, unique selecting component for epidermal T cells. Proceedings of the National Academy of Sciences of the United States of America 108, 3330–3335 (2011). [PubMed: 21300860]
26. Schlenner SM et al. Fate mapping reveals separate origins of T cells and myeloid lineages in the thymus. Immunity 32, 426–436 (2010). [PubMed: 20303297]
27. Wende H et al. The transcription factor c-Maf controls touch receptor development and function. Science 335, 1373–1376 (2012). [PubMed: 22345400]
28. Kashem SW et al. Nociceptive Sensory Fibers Drive Interleukin-23 Production from CD301b+ Dermal Dendritic Cells and Drive Protective Cutaneous Immunity. Immunity 43, 515–526 (2015). [PubMed: 26377898]
29. Laird RM, Laky K & Hayes SM Unexpected role for the B cell-specific Src family kinase B lymphoid kinase in the development of IL-17-producing gammadelta T cells. Journal of immunology 185, 6518–6527 (2010).
30. Eberl G & Littman DR Thymic origin of intestinal alphabeta T cells revealed by fate mapping of RORgammat+ cells. Science 305, 248–251 (2004). [PubMed: 15247480]
31. Visel A et al. ChIP-seq accurately predicts tissue-specific activity of enhancers. Nature 457, 854–858 (2009). [PubMed: 19212405]
32. Powolny-Budnicka I et al. RelA and RelB transcription factors in distinct thymocyte populations control lymphotoxin-dependent interleukin-17 production in gammadelta T cells. Immunity 34, 364–374 (2011). [PubMed: 21419662]
33. Shibata K et al. IFN-gamma-producing and IL-17-producing gammadelta T cells differentiate at distinct developmental stages in murine fetal thymus. Journal of immunology 192, 2210–2218 (2014).
34. Muro R et al. gammadeltaTCR recruits the Syk/PI3K axis to drive proinflammatory differentiation program. The Journal of clinical investigation 128, 415–426 (2018). [PubMed: 29202478]
35. Azzam HS et al. CD5 expression is developmentally regulated by T cell receptor (TCR) signals and TCR avidity. The Journal of experimental medicine 188, 2301–2311 (1998). [PubMed: 9858516]
36. Ito K et al. Different gamma delta T-cell receptors are expressed on thymocytes at different stages of development. Proceedings of the National Academy of Sciences of the United States of America 86, 631–635 (1989). [PubMed: 2463632]
37. Azuara V, Lembezat MP & Pereira P The homogeneity of the TCRdelta repertoire expressed by the Thy-1dull gammadelta T cell population is due to cellular selection. European journal of immunology 28, 3456–3467 (1998). [PubMed: 9842888]
38. Ciofani M, Knowles GC, Wiest DL, von Boehmer H & Zuniga-Pflucker JC Stage-specific and differential notch dependency at the alphabeta and gammadelta T lineage bifurcation. Immunity 25, 105–116 (2006). [PubMed: 16814577]

39. Mombaerts P, Anderson SJ, Perlmutter RM, Mak TW & Tonegawa S An activated lck transgene promotes thymocyte development in RAG-1 mutant mice. Immunity 1, 261–267 (1994). [PubMed: 7889413]
40. Gabrysova L et al. c-Maf controls immune responses by regulating disease-specific gene networks and repressing IL-2 in CD4(+) T cells. Nature immunology 19, 497–507 (2018). [PubMed: 29662170]
41. Vahedi G et al. STATs shape the active enhancer landscape of T cell populations. Cell 151, 981–993 (2012). [PubMed: 23178119]
42. Barros-Martins J et al. Effector gammadelta T Cell Differentiation Relies on Master but Not Auxiliary Th Cell Transcription Factors. Journal of immunology 196, 3642–3652 (2016).
43. Munoz-Ruiz M, Sumaria N, Pennington DJ & Silva-Santos B Thymic Determinants of gammadelta T Cell Differentiation. Trends Immunol 38, 336–344 (2017). [PubMed: 28285814]
44. Tanaka S et al. Sox5 and c-Maf cooperatively induce Th17 cell differentiation via RORgammat induction as downstream targets of Stat3. The Journal of experimental medicine 211, 1857–1874 (2014). [PubMed: 25073789]
45. Rajaram N & Kerppola TK Synergistic transcription activation by Maf and Sox and their subnuclear localization are disrupted by a mutation in Maf that causes cataract. Mol Cell Biol 24, 5694–5709 (2004). [PubMed: 15199128]
46. Yu Q, Sharma A, Ghosh A & Sen JM T cell factor-1 negatively regulates expression of IL-17 family of cytokines and protects mice from experimental autoimmune encephalomyelitis. Journal of immunology 186, 3946–3952 (2011).
47. Lee SY et al. Noncanonical mode of ERK action controls alternative alphabeta and gammadelta T cell lineage fates. Immunity 41, 934–946 (2014). [PubMed: 25526308]
48. Auderset F et al. Notch signaling regulates follicular helper T cell differentiation. Journal of immunology 191, 2344–2350 (2013).
49. Zhang YE Non-Smad pathways in TGF-beta signaling. Cell Res 19, 128–139 (2009). [PubMed: 19114990]
50. Rossi FM, Kringstein AM, Spicher A, Guicherit OM & Blau HM Transcriptional control: rheostat converted to on/off switch. Molecular cell 6, 723–728 (2000). [PubMed: 11030351]
51. Carr TM, Wheaton JD, Houtz GM & Ciofani M JunB promotes Th17 cell identity and restrains alternative CD4+ T-cell programs during inflammation. Nature communications 8, 301 (2017).
52. Ciofani M et al. Obligatory role for cooperative signaling by pre-TCR and Notch during thymocyte differentiation. Journal of immunology 172, 5230–5239 (2004).
53. Morita S, Kojima T & Kitamura T Plat-E: an efficient and s system for transient packaging of retroviruses. Gene Ther 7, 1063–1066 (2000). [PubMed: 10871756]
54. Ramsdell F, Zuniga-Pflucker JC & Takahama Y In vitro systems for the study of T cell development: fetal thymus organ culture and OP9-DL1 cell coculture. Curr Protoc Immunol Chapter 3, Unit 3 18 (2006). [PubMed: 18432973]
55. Dobin A et al. STAR: ultrafast universal RNA-seq aligner. Bioinformatics 29, 15–21 (2013). [PubMed: 23104886]
56. Liao Y, Smyth GK & Shi W featureCounts: an efficient general purpose program for assigning sequence reads to genomic features. Bioinformatics 30, 923–930 (2014). [PubMed: 24227677]
57. Robinson MD, McCarthy DJ & Smyth GK edgeR: a Bioconductor package for differential expression analysis of digital gene expression data. Bioinformatics 26, 139–140 (2010). [PubMed: 19910308]
58. Corces MR et al. An improved ATAC-seq protocol reduces background and enables interrogation of frozen tissues. Nature methods 14, 959–962 (2017). [PubMed: 28846090]
59. Langmead B & Salzberg SL Fast gapped-read alignment with Bowtie 2. Nature methods 9, 357–359 (2012). [PubMed: 22388286]
60. Quinlan AR & Hall IM BEDTools: a flexible suite of utilities for comparing genomic features. Bioinformatics 26, 841–842 (2010). [PubMed: 20110278]
61. Ramirez F et al. deepTools2: a next generation web server for deep-sequencing data analysis. Nucleic acids research 44, W160–165 (2016). [PubMed: 27079975]

62. Li H et al. The Sequence Alignment/Map format and SAMtools. Bioinformatics 25, 2078–2079 (2009). [PubMed: 19505943]

63. Zhang Y et al. Model-based analysis of ChIP-Seq (MACS). Genome biology 9, R137 (2008). [PubMed: 18798982]

64. Heinz S et al. Simple combinations of lineage-determining transcription factors prime cis-regulatory elements required for macrophage and B cell identities. Molecular cell 38, 576–589 (2010). [PubMed: 20513432]

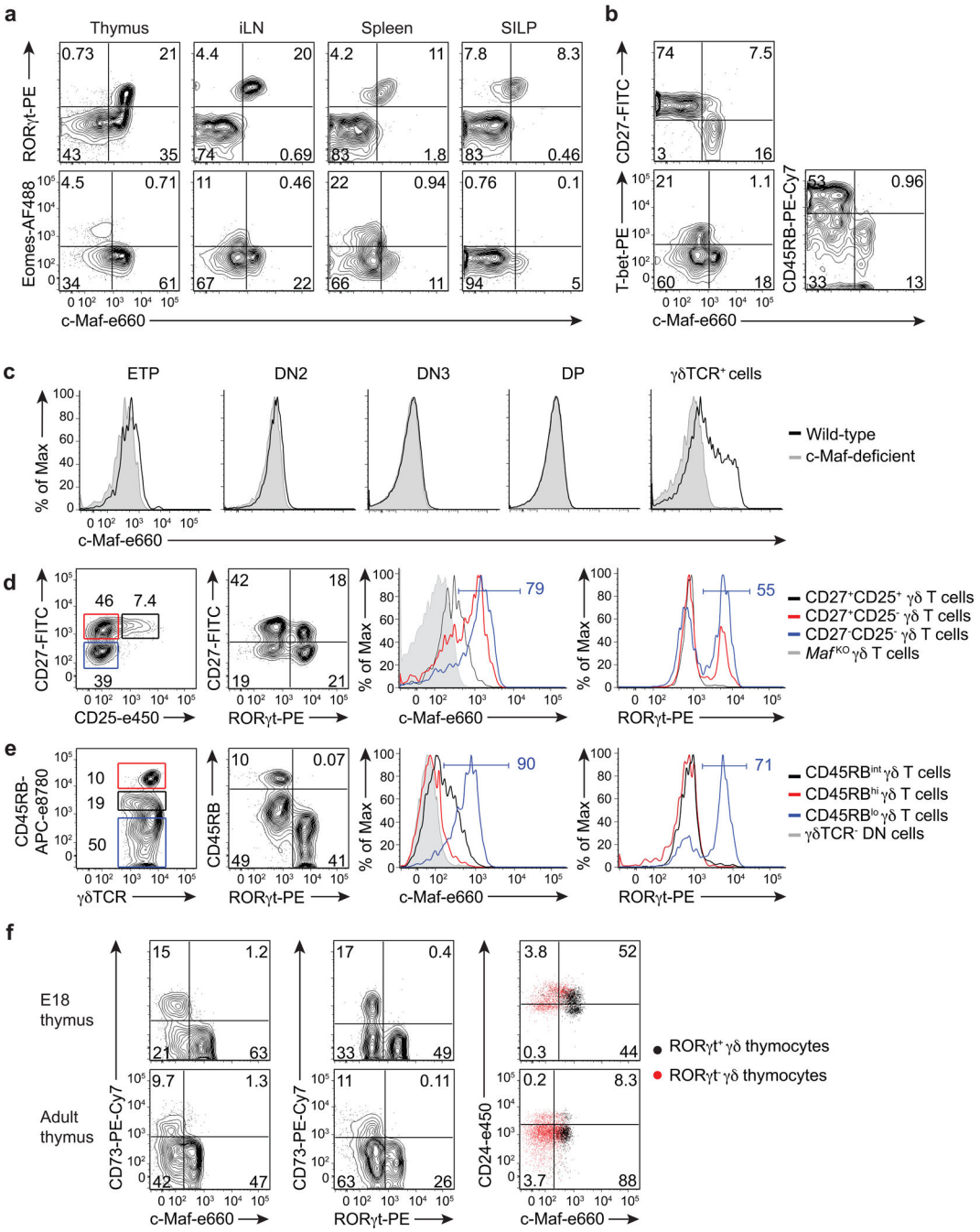

Fig. 1. Selective expression of c-Maf in Tγδ17 cells.

(a) Flow cytometric analysis of transcription factors, gated on CD3ε$^+$γδTCR$^+$ cells from the indicated tissues of wild-type mice. (b) Flow cytometry for c-Maf expression and markers of Tγδ1 cells gated on CD3ε$^+$γδTCR$^+$ cells in the spleen from wild-type mice. (c) Flow cytometric analysis of c-Maf expression in E16 fetal thymic ETP (Lin$^-$CD117$^+$CD25$^-$), DN2 (Lin$^-$CD117$^+$CD25$^+$), DN3 (Lin$^-$CD117$^{lo/-}$CD25$^+$), DP (CD4$^+$CD8$^+$), and γδ T (CD3ε$^+$γδTCR$^+$) cells (black line). Intracellular staining of c-Maf in equivalent *Maf*-deficient subsets (grey filled) represents a negative control. (d, e) Flow cytometry plots gated

on CD3ε$^+$γδTCR$^+$ cells (left), and histograms showing c-Maf and RORγt expression for the indicated γδ T cell subsets in E18 FT (right). Proportions in histograms refer to CD27$^-$CD25$^-$ (d) and CD45RB^{lo} (e) γδ thymocyte subsets (blue). c-Maf-deficient (*Maf*^{KO}) γδTCR$^+$ cells and γδTCR$^-$ DN cells are c-Maf null staining controls. (f) Flow cytometric analysis showing expression of c-Maf relative to CD73 and CD24 maturation markers in E18 fetal and adult thymus gated on CD3ε$^+$γδTCR$^+$ cells. Dot plots delineate RORγt$^+$ (black) and RORγt$^-$ (red) γδ T cells. Data are representative of three independent experiments.

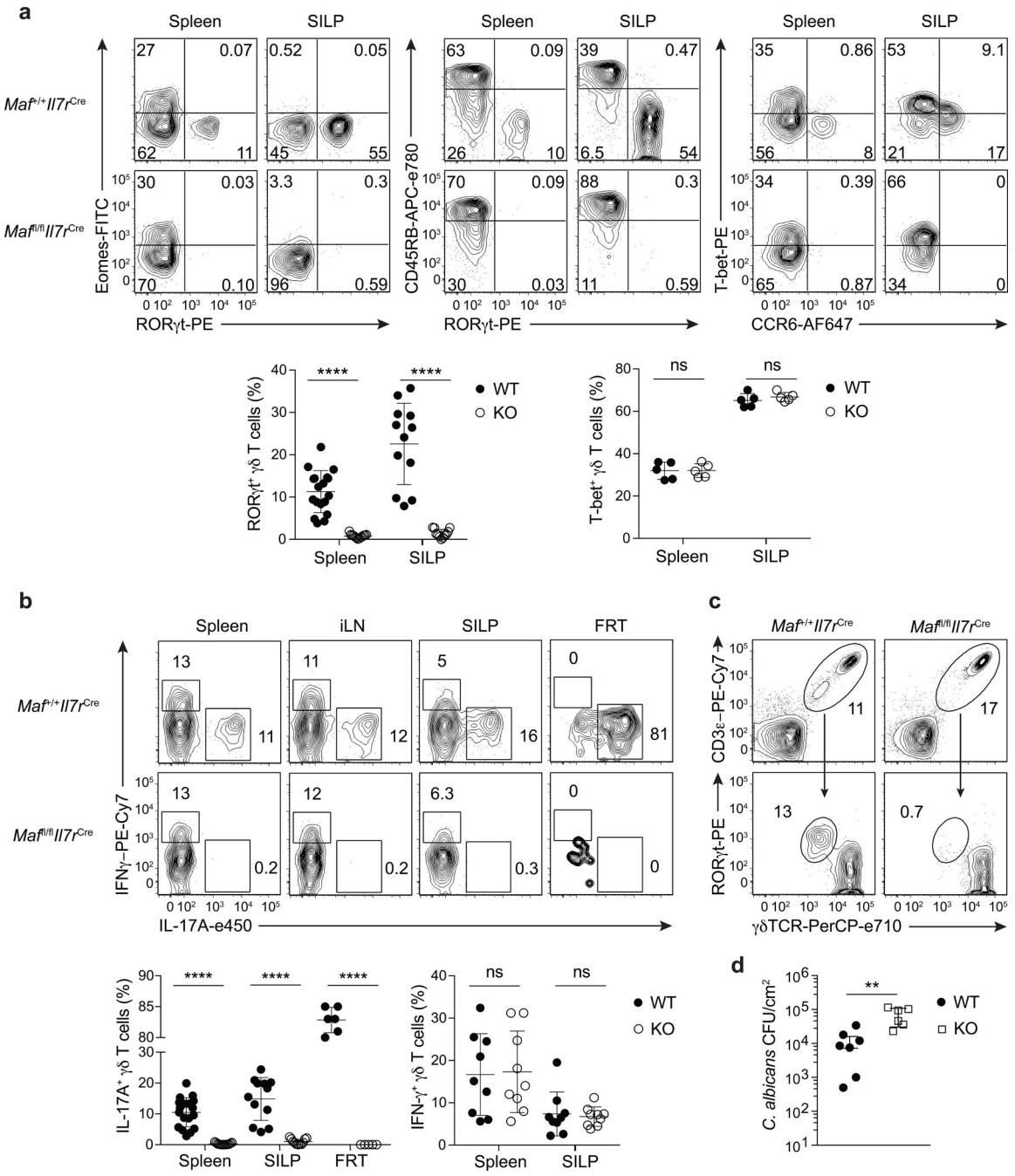

Fig. 2. Selective loss of peripheral Tγδ17 cells in the absence of c-Maf.

(a) Flow cytometric analysis showing Tγδ17 and Tγδ1 subsets in spleen and small intestine lamina propria (SILP) of *Maf*$^{+/+}$*Il7r*^{Cre} (WT) and *Maf*$^{fl/fl}$*Il7r*^{Cre} (KO) mice gated for CD3ε^{+}γδTCR^{+} cells. Summary data showing percentages of RORγt^{+} (n=16 spleen, n=12 SILP per group) and T-bet^{+} cells (n=5 spleen, n=5 SILP per group) among CD3ε^{+}γδTCR^{+} cells for WT and KO mice. (b) Intracellular cytokine production gated on CD3ε^{+}γδTCR^{+} γδ T cells isolated from indicated tissues of WT and KO mice and stimulated *in vitro* for 4h (top). iLN, inguinal lymph node; FRT, female reproductive tract. Percentages of IL-17A^{+} and IFN-

γ^+ cells are graphed (bottom) for WT and KO mice (n=16 spleen, n=12 SILP, n=6 FRT per group). (c) Top: flow cytometry plots gated for total live $CD45^+$ cells isolated from back skin from WT and KO mice. Bottom: plots additionally gated for $CD3\varepsilon^+$ and $\gamma\delta TCR^+$. (d) Number of *C. albicans* colony forming units (CFU) per cm^2 of homogenized back skin harvested 3 days post infection from WT (n=7) and KO (n=6) mice combined from two independent experiments. Each data point represents an individual mouse. Population distribution data (a), (b), (c) are representative of three independent experiments. All results represent mean ± SEM and are analyzed by unpaired two-tailed Student's t-test. ** $p<0.01$; **** $p<0.0001$. ns, not significant.

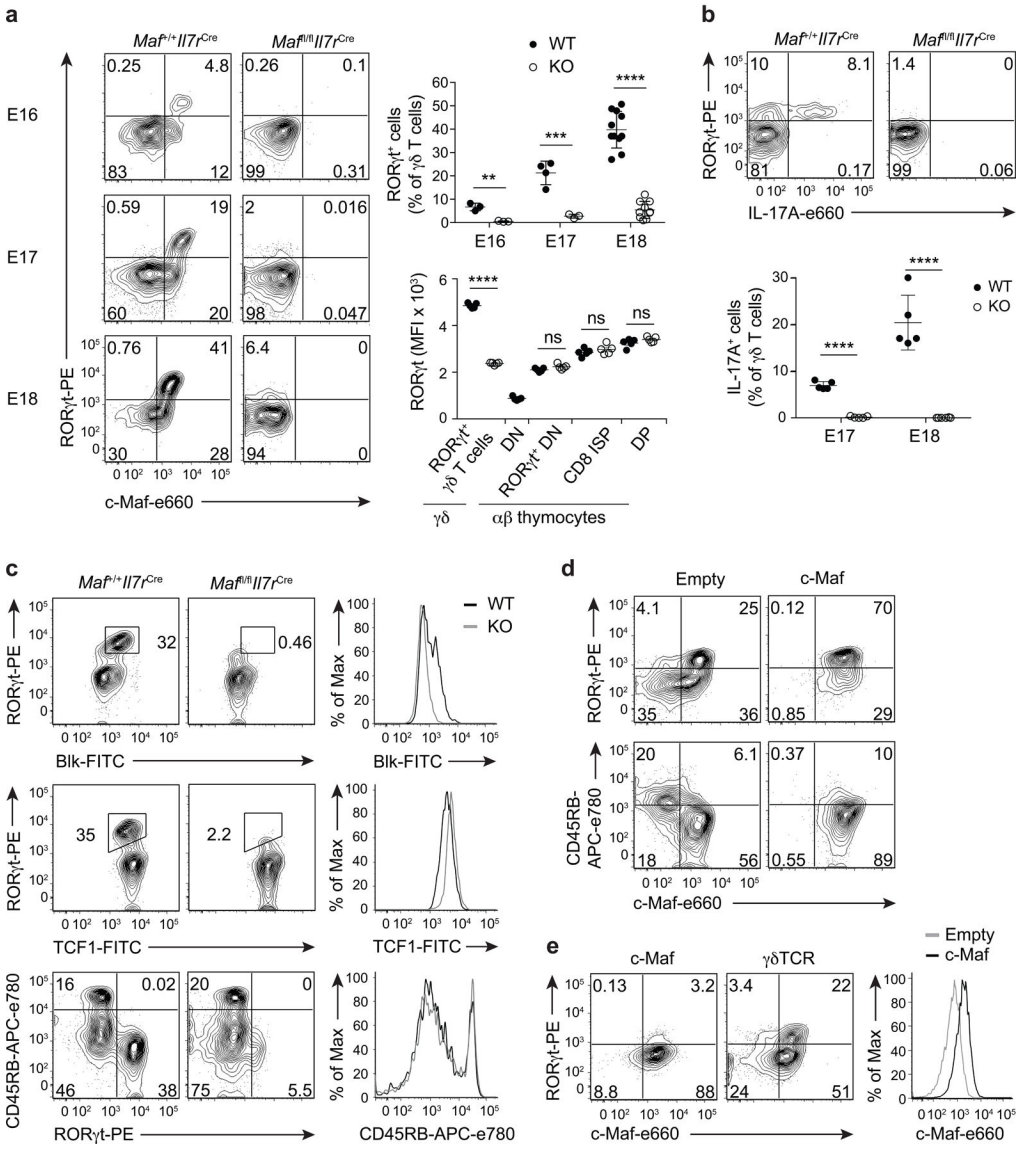

Fig. 3. c-Maf is required for Tγδ17 differentiation.

(a) Left: Flow cytometric analysis of *Maf*$^{+/}$*Il7r*^{Cre} (WT) and *Maf*$^{fl/fl}$*Il7r*^{Cre} (KO) γδ fetal thymocytes at E16, E17, and E18 (gated CD4^{-}CD8^{-}CD3ε^{+}γδTCR^{+}). Right: Percentage of RORγt^{+} cells among γδ T cells at E16 (n=4), E17 (n=4), and E18 (n=11) (top). Mean fluorescence intensity (MFI) of RORγt in E18 FT populations (bottom) of RORγt^{+} γδ T cells (CD4^{-}CD8^{-}CD3ε^{+}γδTCR^{+}), DN (CD4^{-}CD8^{-}CD3ε^{-}), CD8 immature single positive (ISP; CD4^{-}CD8^{+}CD3ε^{-}), and DP (CD4^{+}CD8^{+}) cells (n=5). (b) IL-17A production following *in vitro* stimulation of WT or KO fetal thymocytes gated for E17 γδ T cells (CD3ε^{+} δTCR^{+}; top). Graph displays the proportion of WT and KO E17 or E18 γδ T cells producing IL-17A (n=5 biological replicates per group). Data combined from three independent experiments. (c) Plots and histograms gated for CD4^{-}CD8^{-}CD3ε^{+}γδTCR^{+} cells in E18 FT WT and KO. (d) Developmental progression of *in vitro*-derived DN3 thymocytes transduced with an empty (Thy1.1^{+}) or a c-Maf expression vector and cultured

on OP9-DL1 stroma for 13 days. Plots gated for Thy1.1^{+} transduced γδ T cells. (e) RORγt expression following differentiation of c-Maf- or γδTCR-transduced *Rag1*$^{-/-}$ DN3 thymocytes with OP9-DL1 cells for 13 days (left). Histogram comparing c-Maf- versus empty vector-transduced *Rag1*$^{-/-}$ DN3 cultures gated for Thy1.1^{+}CD4^{-}CD8^{-} cells. All panels (a-e) are representative of at least three independent experiments. All results represent mean ± SEM. ** p<0.01; *** p< 0.001; **** p<0.0001; ns, not significant (two-tailed unpaired Student's t-test).

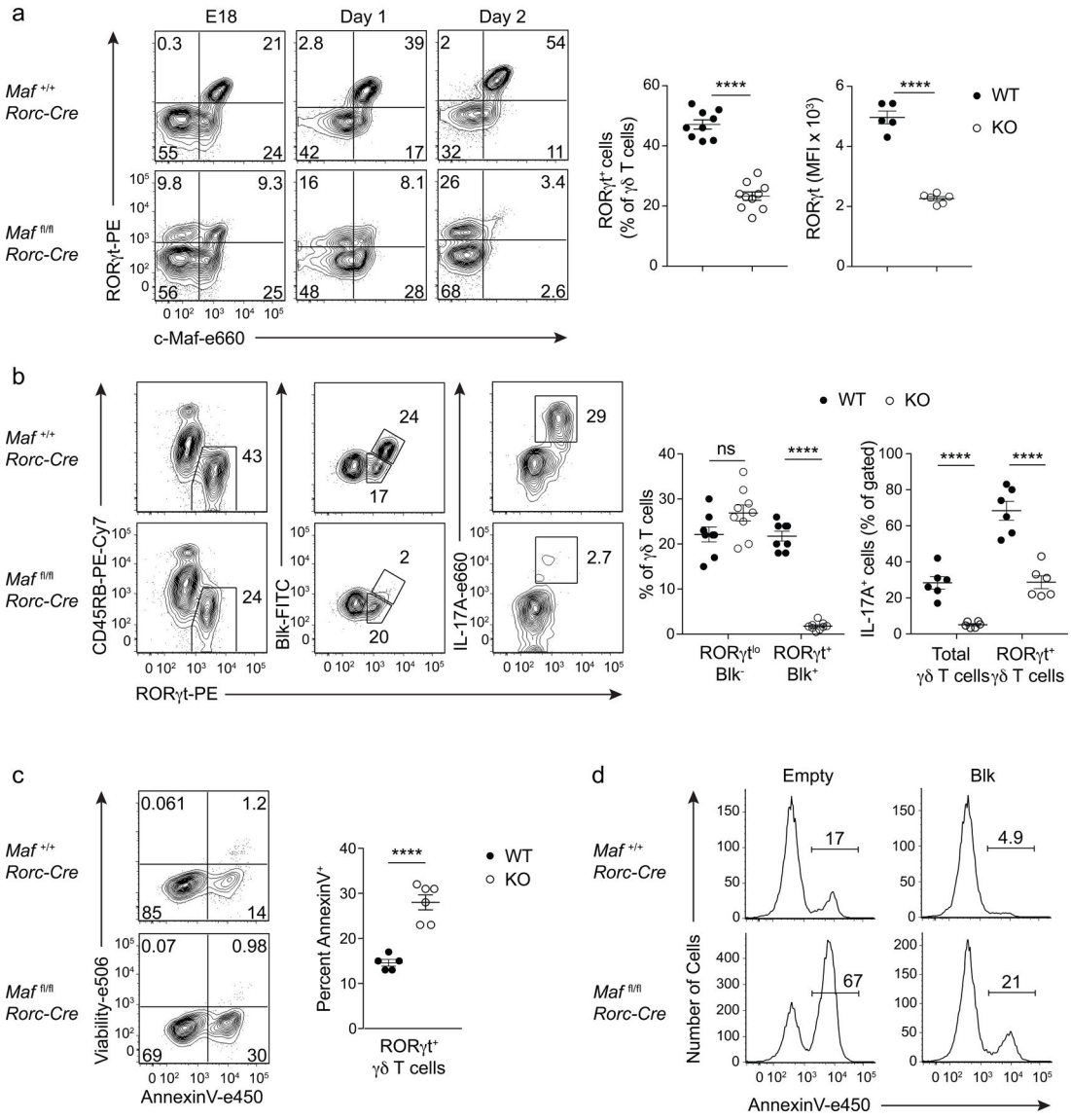

Fig. 4. c-Maf maintains Tγδ17 cell features.

(a) Left: flow cytometric analysis of γδ fetal thymocytes from *Maf*$^{+/+}$*Rorc*-Cre (WT) and *Maf*$^{fl/fl}$*Rorc*-Cre (KO) at E18 and neonatal days 1 and 2. Plots gated for γδ T cells ($CD4^-CD8^-CD3\varepsilon^+\gamma\delta TCR^+$). Right: summary graph for the percentage of RORγt$^+$ cells among γδ T cells at neonatal day 2 (WT n=9, KO n=10, representative of three independent experiments), and for the mean fluorescence intensity (MFI) of RORγt for RORγt$^+$ γδ thymocytes (WT n=5, KO n=6). (b) Plots are gated for γδ thymocytes (as in a) isolated from *Maf*$^{+/+}$*Rorc*-Cre (WT) and *Maf*$^{fl/fl}$*Rorc*-Cre (KO) day 1 neonates. Graphs depict percent of γδ thymocytes that are (left) RORγt^{lo}Blk$^-$ and RORγt$^+$Blk$^+$ (WT n=8, KO n=9 biological replicates), and (right) IL-17A$^+$ cells following *in vitro* stimulation as a proportion of total γδ or RORγt$^+$ γδ thymocytes (n=6 per group). Data compiled from two independent experiments. (c) Flow cytometric plots and summary graph show the percent of AnnexinV$^+$ cells among specified neonatal day 1 γδ thymocyte populations (WT n=5, KO n=6). Data

compiled from two independent experiments. (d) Flow cytometry plots displaying the proportion of AnnexinV^{+} transduced neonatal day 1 CD45RB^{lo} γδ T cells (gated CD4^{-}CD8^{-}CD3ε^{+}γδTCR^{+}Thy1.1^{+}) following 2 days of OP9-DL1 culture. Data representative of two experiments. For all graphs, results represent mean ± SEM. ns, not significant; **** $p<0.0001$ (two-tailed unpaired Student's t-test).

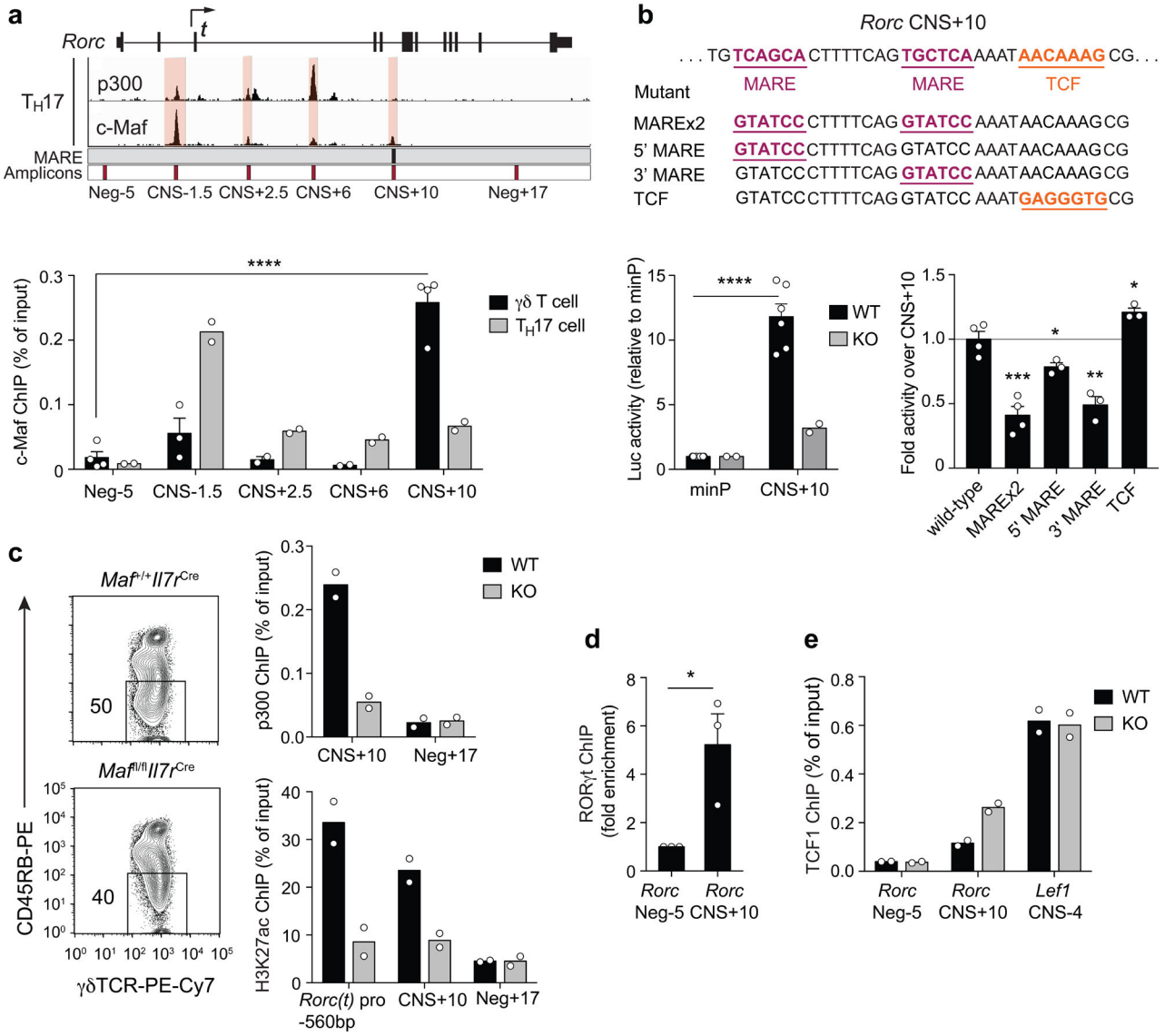

Fig. 5. c-Maf controls the regulatory status of the *Rorc* locus in γδ thymocytes.

(a) ChIP-Seq for c-Maf and p300 occupancy at the *Rorc* locus in *in vitro* polarized Th17 cells (top). ChIP-qPCR of c-Maf binding in the *Rorc* locus in E18 CD45RB^{lo} γδ T cells and *in vitro* polarized Th17 cells (48h; bottom; n=4 for comparison, n=2 for all others). CNS, conserved non-coding sequence; t, *Rorc(t)* exon 1 and transcription start (arrow). Neg-5 and Neg+17 are negative control regions devoid of MARE sites. (b) Luciferase reporter assay of enhancer activity for *Rorc* CNS+10 in CD45RB^{lo} γδ T cells sort purified from day 11 OP9-DL1 cultures of *Maf*$^{+/+}$*Il7r*^{Cre} (WT) and *Maf*$^{fl/fl}$*Il7r*^{Cre} (KO) fetal liver progenitor cells (left, bottom; n=6 for WT, n=2 for KO). Activity of CNS+10 MARE and TCF1 binding site mutants relative to unmodified sequence assayed in day 11 C57BL/6 fetal liver-derived CD45RB^{lo} γδ T cells (Right bottom; n=4 CNS+10 and MAREx2, n=3 for individual MAREs and TCF). Representative of three experiments. Mutations in sequence are underlined (top). (c, e) Sort strategy for ChIP assay performed for CD45RB^{lo} γδ T cells

isolated from *Maf*$^{+/+}$*Il7r*^{Cre} (WT) and *Maf*$^{fl/fl}$*Il7r*^{Cre} (KO) E18 FT. ChIP qPCR for p300 and H3K27ac (c), and TCF1 (e) displayed as percent of input DNA for the *Rorc* locus (n=2 per group for c and e). (d) RORγt ChIP for *Rorc* locus CNS+10 performed for E18 CD45RB^{lo} γδ T cells and represented as fold enrichment relative to a negative control region (Neg-5) located 5kb upstream of the *Rorc(t)* transcription start site (n=3). Data compiled from (a) four, (b, c, e) two, (d) three independent experiments using mean ± SEM for (a, b, and d). For all graphs, * $p<0.05$, **** $p<0.0001$ unpaired two-tailed Student's t-test (a, d).

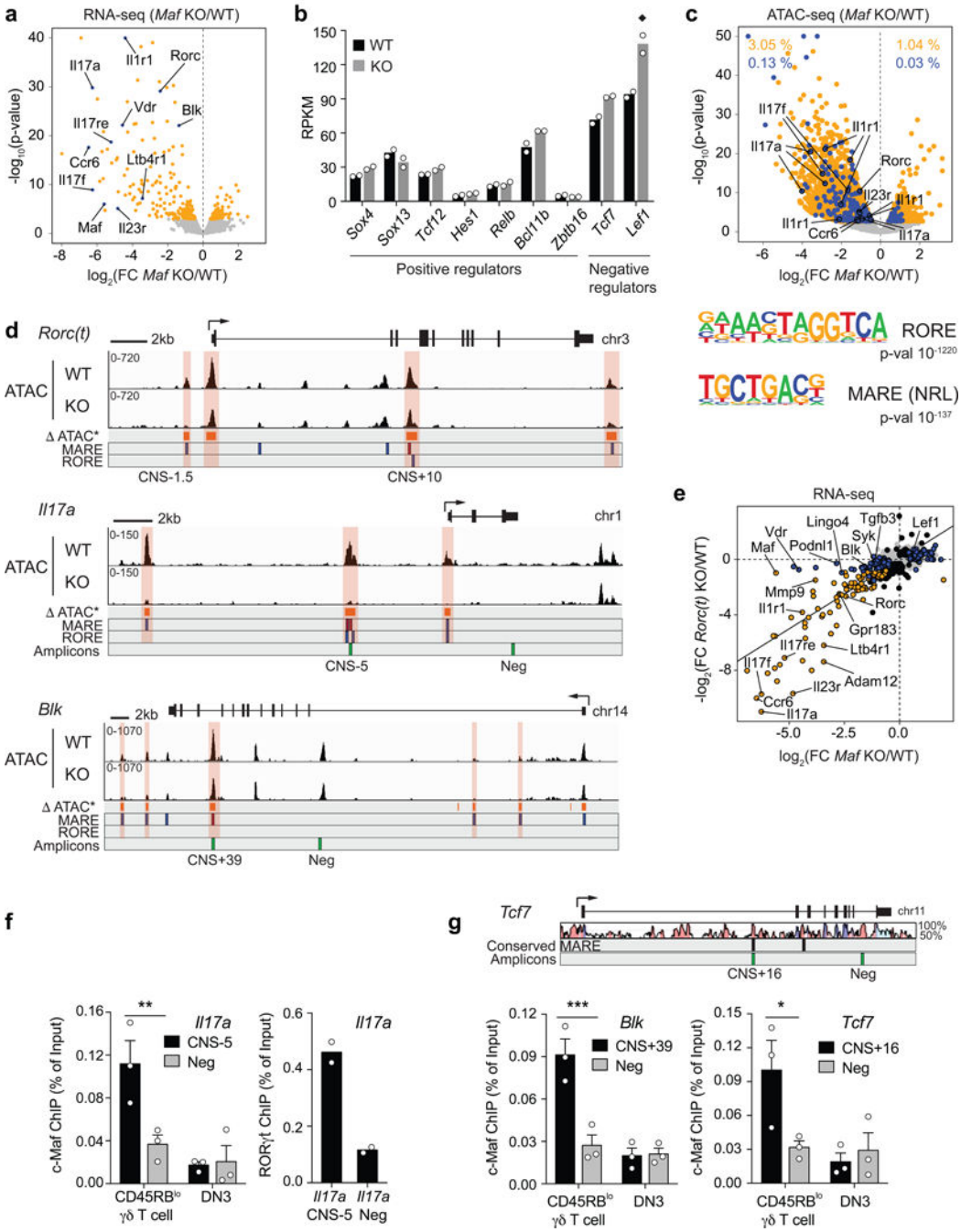

Fig. 6. c-Maf is essential for Tγδ17 programming.

(a) Differential mRNA expression in *Maf*$^{+/+}$*Il7r*^{Cre} (WT) and *Maf*$^{fl/fl}$*Il7r*^{Cre} (KO) E17–18 CD25^{-}CD27^{-} γδ thymocytes displayed as a volcano plot of log2 fold change vs. the –log10(p-value) for each gene. Genes considered significant (FDR < 0.05) are in orange, while select Tγδ17-associated genes are in blue. *p*-value capped at 10^{-40}. (b) RNA expression values for known Tγδ17 transcriptional regulators from (a) RPKM, reads per kilobase million. ♦, significant differential expression at FDR < 0.05. (c) Differential ATAC-seq analysis in Maf WT and KO E17–18 CD24^{+}CD45RB^{lo}TCRγδ^{+}CD3ε^{+} cells. Regions

having significantly differential accessibility (FDR < 0.05) are in orange. Significant regions within 10 kb up- or down-stream of a differentially-expressed gene (*Maf* KO) are further highlighted in blue, with select type-17-associated regions annotated with gene symbols, *p*-value capped at 10^{-50}. Proportion DA of total significant ATAC peaks indicated for each half (top). Results of *de novo* motif enrichment analysis comparing differential ATAC peaks (FDR<0.05) against non-differential, with the two most-enriched motifs shown (bottom). (d) ATAC-seq tracks at select loci displayed using IGV for *Maf* WT and KO $CD24^{+}CD45RB^{lo}$ γδ thymocytes. ΔATAC* track and shading denotes DA regions (FDR<0.05). MARE and RORE indicated in blue, MARE with human conservation in red, location of qPCR amplicons in green. (e) Comparison of differential expression log2 fold-change by RNA-seq in *Maf* KO and *Rorc(t)* KO E17–18 $CD27^{-}CD25^{-}$ γδ thymocytes. Genes differentially expressed (FDR < 0.05) in *Maf* KO (blue), *Rorc(t)* KO (black), or both (orange) are highlighted, with select type 17 program genes annotated. (f) c-Maf and RORγt ChIP-qPCR analysis of the *Il17a* locus, and (g) c-Maf ChIP-qPCR of the *Blk* and *Tcf7* loci for WT and KO E18 $CD45RB^{lo}$ γδ T cells Number of biological replicates per group for (a-d) n=2, (e) n=4, (f, g) n=3. Mean ± SEM used. * p<0.05, ** p<0.01, *** p<0.001, two-way ANOVA with Fisher's LSD post-test (f left, g).

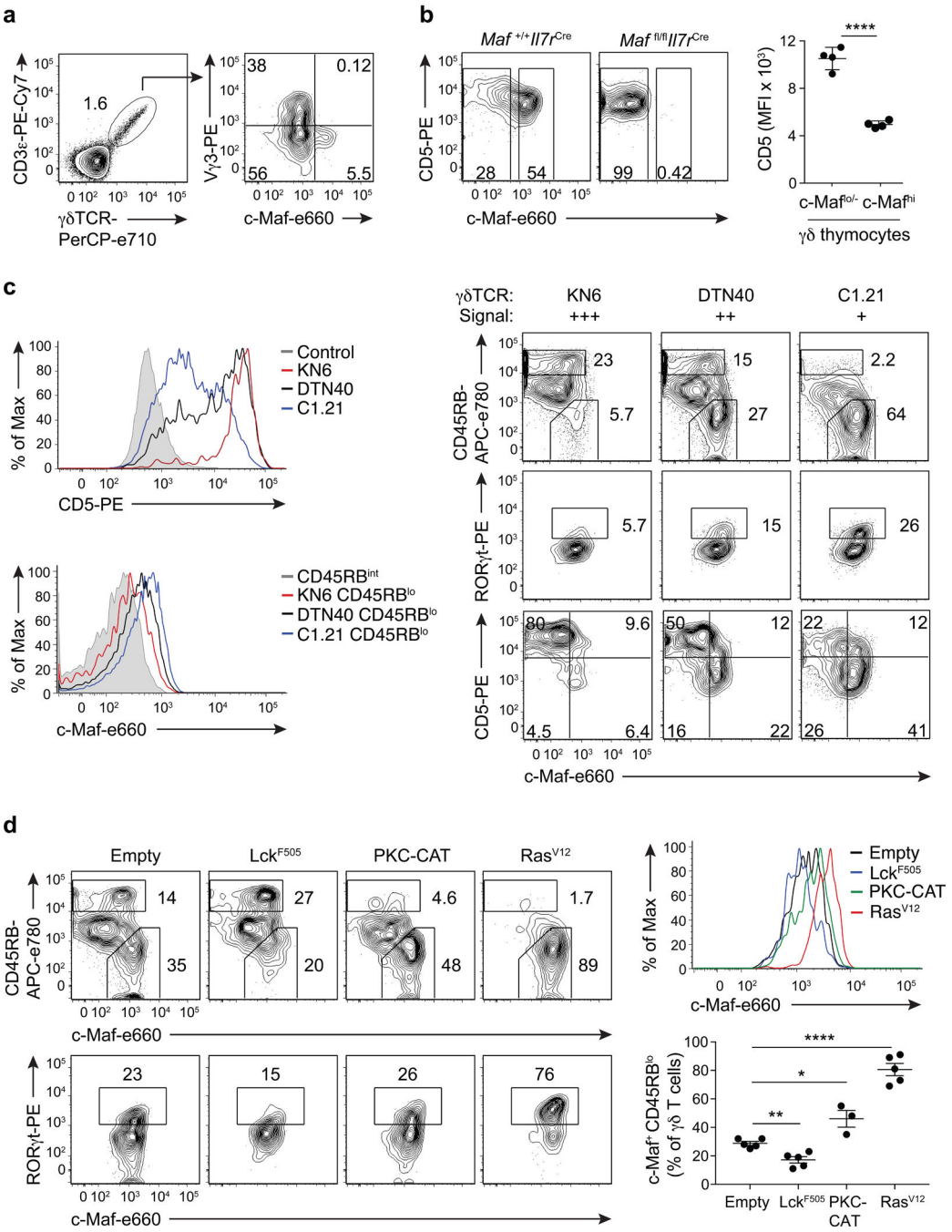

Fig. 7. TCR signals modulate c-Maf expression during γδ diversification.

(a) Flow cytometry plots shown for E15 fetal thymus and gated as indicated. Representative of three experiments. (b) Flow cytometry plots depict E18 FT gated for γδ T cells ($CD4^-CD8^-CD3\varepsilon^+\gamma\delta TCR^+$); $Maf^{fl/fl}Il7r^{Cre}$ cells are used to gate c-Maf positive versus negative cells. Graph of CD5 mean fluorescence intensity (MFI) shown for c-Maf^+ and c-Maf^- γδ T cells (n=5). Data representative of three experiments. (c) Flow cytometric analysis of purified γδTCR-transduced culture-derived $Rag1^{-/-}$ DN2 cells after 7 days of OP9-DL1 culture. Histograms and contour plots are gated for $CD4^-CD8^-\gamma\delta TCR^+$

transduced cells. In RORγt versus c-Maf plots, cells were additionally gated for $CD45RB^{lo}$ expression. Data is representative of three independent experiments. (d) Flow cytometric analysis for purified active kinase-transduced GFP^+ DN2 cells after 7 days of OP9-DL1 culture. Histograms and contour plots are gated for $CD4^-CD8^-CD3\varepsilon^+\gamma\delta TCR^+GFP^+$ transduced cells. In RORγt versus c-Maf plots, cells were additionally gated on $CD45RB^{lo}$ expression. Graph of the proportion of $c\text{-}Maf^+CD45RB^{lo}$ summarizes at least three independent experiments and n=5 for all conditions besides n=3 for PKC-CAT. For all graphs, mean ± SEM. ns, not significant; * $p<0.05$, ** $p<0.01$, **** $p<0.0001$, unpaired two-tailed Student's t-test.